

Rethinking Weight-Averaged Model-merging

Hu Wang¹, Congbo Ma¹, Ibrahim Almakky¹, Ian Reid¹, Gustavo Carneiro², Mohammad Yaqub¹

¹Mohamed bin Zayed University of Artificial Intelligence, UAE

²University of Surrey, Guildford, United Kingdom

Abstract

*Model-merging has emerged as a powerful approach in deep learning, capable of enhancing model performance without any training. However, the underlying mechanisms that explain its effectiveness remain largely unexplored. In this paper, we investigate this technique from three novel perspectives to empirically provide deeper insights into why and how weight-averaged model-merging works: (1) we examine **the intrinsic patterns captured by the learning of the model weights**, through the visualizations of their patterns on several datasets, showing that these weights often encode structured and interpretable patterns and that is the essential why model-merging can work; (2) we mathematically and empirically investigate model ensemble merging strategies based on **averaging on weights versus averaging on features**, providing detailed analyses across diverse architectures and datasets; and (3) we explore **the impact on model-merging prediction stability in terms of changing the parameter magnitude**, revealing insights into the way of weight averaging works as regularization by showing the robustness across different parameter scales. Our findings shed light on the “black box” of weight-averaged model-merging, offering valuable insights and practical recommendations that advance the model-merging process. The code is available at <https://github.com/billhhh/Rethink-Merge>.*

1. Introduction

Model-merging can combine multiple independently trained models into a single, effective model without introducing extra inference computations. This family of approaches has been applied in contexts such as natural language processing [38], computer vision [16], and their sub-areas (e.g. federated learning [32], distillation [13], adversarial learning [2, 44] and large language model [22, 45]), where the ability to merge models effectively can lead to largely improved models’ performance, efficiency, and flexibility in deployment. Despite the

practical importance of model-merging, there has been limited research on the investigation of the underlying factors that make it effective.

This research gap motivates the need to innovatively explore the underlying principles of why and how the family of weight-averaged model-merging methods can work. In this paper, we bridge this gap by providing a comprehensive analysis of weight-averaged model-merging from the following three key perspectives:

- An examination of the patterns contained in the model weights through the visualization of the patterns present in both linear layers as classifiers or inside deep learning models used on multiple datasets. Results reveal that clear and structured patterns emerge within the weights, suggesting that weight averaging can be seen as a linear vector combination, which contributes to the success of merging models via weight operations;
- An investigation of averaging on weights versus averaging on features strategies allows us to evaluate the relative effectiveness and limitations of model-merging and traditional model ensembles across multiple architectures and datasets, uncovering distinct benefits and behaviors;
- An exploration of the robustness of model-merging predictions with respect to different weight magnitudes/variances, which provides insights into the model-merging works as a type of model regularization.

Based on our viewpoints and findings, we conclude with useful proposals to provide a good reference for the community.

2. Related Work

In recent years, model-merging [3, 21, 23, 25, 28, 37] has attracted growing interest. This approach has led to a range of methods focused on merging weights from independently trained models to enhance model performance or generalization. For example, Wortsman et al. [35] proposed an approach of averaging, or greedily averaging, the parameters from various models to yield “Model Soups” that show more accurate performance than the original models used to produce the “soup” but without introducing more com-

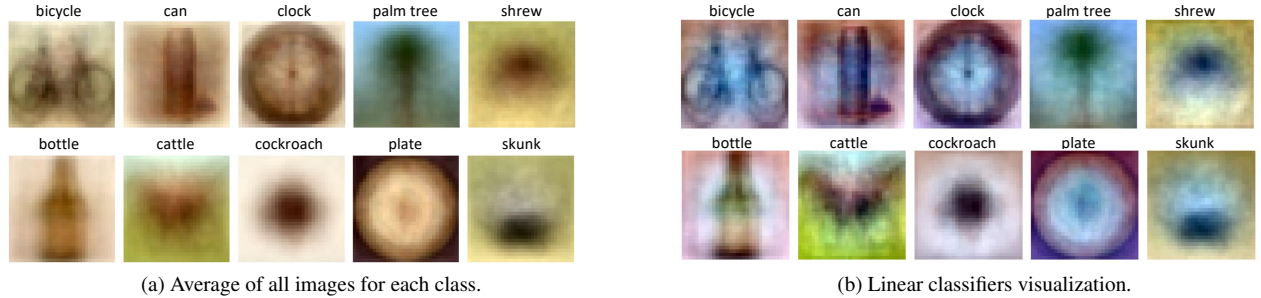


Figure 1. Average of all images for each class (a) and the linear classifier visualization for each class on Cifar100 [14] dataset (b). We train a single linear classifier for all classes then wrap it back to the size of input images. The detailed experimental analysis is in Sec. 6.1.

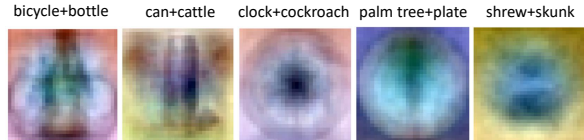


Figure 2. Merge the linear classifiers for the first 5 classes (within the above 10 classes) with the last 5 classes on Cifar100. It interprets the reason why the model-merging techniques can work as they essentially operate the templates contained in model weights.

putations into inference. Further, Yadav et al. proposed Ties-Merging [36] based on parameter averaging by considering conflicts between the model weights, allowing for smooth parameter merging across models. Some other approaches [1, 6, 12] address the problem from a different perspective, focusing on taking weight merging operations via finding a good way to interpolate on the loss basins. Zipit [27] takes one step ahead from Git Re-Basin [1] to align weights from inter-model and intra-model based on the alignment of features between merging models. Yu et al. [41] proposed a DARE model to combine models trained on domain-specific data to create a domain-agnostic model-merging that generalizes well across diverse distributions. This approach ensures that domain knowledge is preserved while enhancing the model’s ability to generalize across different tasks. Beyond model-merging, other techniques, such as mode connectivity path ensembles [8], analyze pathways in the parameter space between models. By identifying optimal modes along these paths, these models help improve the performance after merging. Fisher Merging [19] selects parameters that approximately maximize the joint likelihood of the models’ parameter posteriors.

Despite these advances, research into the underlying mechanisms that make model-merging effective remains limited. This gap in understanding serves as the motivation for our paper. To focus on a specific scope, we aim to offer a thorough analysis from mathematical and empirical perspectives of weight-averaged model-merging different from

the study in [35], which serves as the foundation work for the area.

3. The Patterns Contained in Model Weights

In this section, we will explain the reason why does the weight-averaged model-merging work via the analysis of their weights from the perspective of template matching (an example is shown Fig. 1 and Fig. 2 for a linear model; for nonlinear models, visualizations can be found in the supplementary materials). Specifically, we explain the reason that the weights can be viewed as templates learned from the data and build connections with an inner product which is a widely explored operation in neural networks. By treating the weights as templates, it is understandable that operations in weight space as efforts to manipulate feature representations.

3.1. Connections Between Inner Product and Template Matching

The weights of the model can be interpreted as templates or prototypes for the respective class activations and it has a deep connection with machine learning. A couple of decades ago, Adaboost [7] contained heuristically designed patterns such as HAAR features [31], which are simple hand-crafted filters that capture edges / lines / other low-level image features through weighted sums and differences in pixel intensities. During training, Adaboost iteratively adjusts the weights of weak classifiers to improve their performance on misclassified examples.

In a linear classification, once the weights are learned, we wrap it back to have the same size with the input images. Take Cifar100 for instance, each image within the dataset is $32 \times 32 \times 3$, if we flatten it and it will become a 3072×1 vector; the weight matrix size is 100×3072 without considering bias; in this case, each row of the weight matrix corresponds to each class to be classified and thus each row vector (1×3072) can be wrapped back to $32 \times 32 \times 3$ with the same size of the original images. The learned weight matrix serves as simplified templates that represent each class

within the data, as shown in Fig. 6.1.

A key mechanism enabling these templates to operate effectively is the use of inner products to apply them to the input data. When an image is presented to the model, its activation is determined by the inner product between the image features and per class weight vector. For each class, which weight vector yields the highest activation is selected as the predicted class of that vector, indicating that the “template” aligns (or similar to) the input image most closely. This phenomenon also holds for deeper networks, but differently from the linear classifier, weight templates in each layer are learned to detect different features that contribute the most towards the objectives (e.g. in the lower layer, low level features, e.g. edge / line features, are tend to be learned). The averaging operation in the weight space represents as Fig. 2, which can be seen as the Mixup [42] operation in the weight space. Therefore, the linear combinations in the weight space has a similar effect as in the feature space. This also explains why recent research [4, 11, 43, 46] applies “model arithmetic” on multiple models in the weight space can achieve the effect of feature arithmetic as Word2vec [20].

Extending to model-merging, the combined model retains the diverse patterns learned from each ingredient model. The model after merging can work more effectively than individuals because it represents a broader set of learned templates, increasing the chances that for any given input the merged model provides a good match. Also, it may provide an effect of regularization by merging different sophisticatedly learned patterns, which enhances the model robustness and generalization ability.

3.2. Formal Representation from the Perspective of Template Matching

As the inner product computation adopted in linear classification is essentially a similarity measurement, so for a linear classifier, each row of the weight vector $\mathbf{w} \in \mathbb{R}^n$ can be interpreted as a template for a particular class. The input vector is denoted as $\mathbf{x} \in \mathbb{R}^n$. The inner product between \mathbf{w} and \mathbf{x} measures the alignment between them:

$$\mathbf{w} \cdot \mathbf{x} = \sum_{i=1}^n w_i x_i = \|\mathbf{w}\| \|\mathbf{x}\| \cos \theta, \quad (1)$$

where $\|\mathbf{w}\|$ and $\|\mathbf{x}\|$ are the norms of \mathbf{w} and \mathbf{x} , and θ is the angle between the two vectors. When $\theta = 0$, then $\cos \theta = 1$, which means that we have $\mathbf{w} \cdot \mathbf{x} = \|\mathbf{w}\| \|\mathbf{x}\|$, resulting in a weight matrix \mathbf{w} that perfectly matches the input \mathbf{x} , as the inner product in (1) is maximized when the template \mathbf{w} is perfectly aligned with the input \mathbf{x} . On the other hand, when $\theta \neq 0$, then $\cos \theta < 1$, which means that the template and image features become misaligned. This mechanism also applies for the layers within deep learning models. The visualization of deep models can be found in the supplementary materials.

Proposal 1: The analyses above and the experimental study in Sec. 6.1 show weight matrices contain generalizable template information. If in practice, the merged model’s performance is suboptimal, more attention should be directed toward resolving conflicts within the individual learned patterns in the weights.

4. Averaging on Weights vs. Averaging on Features

Averaging on weights (model-merging) and *Averaging on features* (model ensembling) are two different ways to aggregate knowledge from multiple models without retraining. These methods have distinct properties and lead to different testing behaviors. In this section, we explore the differences between these two approaches and analyze their effects on the model effectiveness and efficiency, one example experiment is shown in Fig. 3.

4.1. Linear Model Scenarios

Averaging on Weights. Assuming that our model only contains linear layers, averaging on weights can be referred to as a process where, given two weight matrices \mathbf{W}_1 and \mathbf{W}_2 , we compute their average first, and then apply the result to the input feature vector \mathbf{x} :

$$\overline{\mathbf{W}} = \frac{1}{2} (\mathbf{W}_1 + \mathbf{W}_2) \quad (2)$$

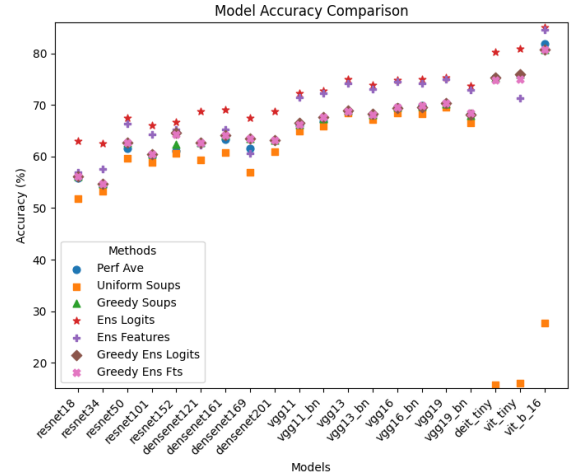


Figure 3. The 10 model-merging/ensemble accuracy comparison between different architectures on Cifar100. Comparison between averaging on Weights (Uniform Soups, Greedy Soups), averaging on features (Ens Logits, Ens Features, Greedy Ens Logits, Greedy Ens Features) and original model performance (Performance Average) on Cifar100 using many different deep learning architectures, including CNNs and ViTs. The detailed experimental analysis is in Sec. 6.2.

The resulting output feature vector is then computed as:

$$\bar{\mathbf{h}} = \overline{\mathbf{W}}\mathbf{x} = \frac{1}{2}(\mathbf{W}_1 + \mathbf{W}_2)\mathbf{x} = \frac{1}{2}(\mathbf{W}_1\mathbf{x} + \mathbf{W}_2\mathbf{x}). \quad (3)$$

Since both \mathbf{W}_1 and \mathbf{W}_2 represent linear transformations, the overall transformation remains linear. When no activation function is involved, this method is mathematically equivalent to averaging on features, as discussed in the next subsection.

Averaging on features involves first applying each weight matrix \mathbf{W}_1 and \mathbf{W}_2 to the input \mathbf{x} separately, with:

$$\mathbf{h}_1 = \mathbf{W}_1\mathbf{x}, \quad \mathbf{h}_2 = \mathbf{W}_2\mathbf{x}, \quad (4)$$

and then averaging the resulting outputs:

$$\bar{\mathbf{h}}' = \frac{1}{2}(\mathbf{h}_1 + \mathbf{h}_2) = \frac{1}{2}(\mathbf{W}_1\mathbf{x} + \mathbf{W}_2\mathbf{x}). \quad (5)$$

In the context of linear operations, the methods in (3) and (5) are equivalent and yield the same result $\bar{\mathbf{h}} = \bar{\mathbf{h}}'$.

4.2. Non-linear Model Scenarios

The equivalence between averaging on weights or on features breaks when non-linear activation functions $\phi(\cdot)$, such as ReLU or Sigmoid, are involved. In the case of averaging on weights, the non-linear activation is applied after averaging the weight matrices:

$$\bar{\mathbf{h}} = \phi(\overline{\mathbf{W}}\mathbf{x}) = \phi\left[\frac{1}{2}(\mathbf{W}_1 + \mathbf{W}_2)\mathbf{x}\right] = \phi\left[\frac{1}{2}(\mathbf{W}_1\mathbf{x} + \mathbf{W}_2\mathbf{x})\right]. \quad (6)$$

When averaging on features, the activation function is applied to each output feature independently:

$$\mathbf{h}_1 = \phi(\mathbf{W}_1\mathbf{x}), \text{ and } \mathbf{h}_2 = \phi(\mathbf{W}_2\mathbf{x}). \quad (7)$$

The final output is then the average of these activated features:

$$\bar{\mathbf{h}}' = \frac{1}{2}(\mathbf{h}_1 + \mathbf{h}_2) = \frac{1}{2}[\phi(\mathbf{W}_1\mathbf{x}) + \phi(\mathbf{W}_2\mathbf{x})]. \quad (8)$$

In such a case, the equivalency between $\bar{\mathbf{h}}$ and $\bar{\mathbf{h}}'$ seen in the linear models may not hold for non-linear models. Take ReLU for instance, if elements of $\mathbf{W}_1\mathbf{x}$ and $\mathbf{W}_2\mathbf{x}$ exhibit totally opposite activations (same absolute values but with different signs), where their average will tend towards zero, leading to large loss of information after the non-linear activation. Therefore, averaging on weights tends to smooth out the contributions from \mathbf{W}_1 and \mathbf{W}_2 , which can be beneficial in certain scenarios by reducing variance or providing a regularizing effect. However, this smoothing may also lead to a loss while extracting fine-grained details. In contrast, averaging on features allows each weight matrix to independently influence the final output after activation. However, averaging on features (model ensemble) increases the computational costs linearly with the number of ensemble models, while averaging on weights (model-merging) does not suffer. The FLOPs of models considered in the paper can be found in the supplementary materials.

Proposal 2: From the analyses above and the experimental study shown in Sec. 6.2, averaging on features can generally produce stronger expressive ability than averaging on weights. However, the averaging on weights can show promising performance without introducing extra inference computational overhead. Hence, this forms a trade-off between computation cost and model performance while deciding between model-merging or model ensembling.

5. The Model Predictions and Weight Magnitudes

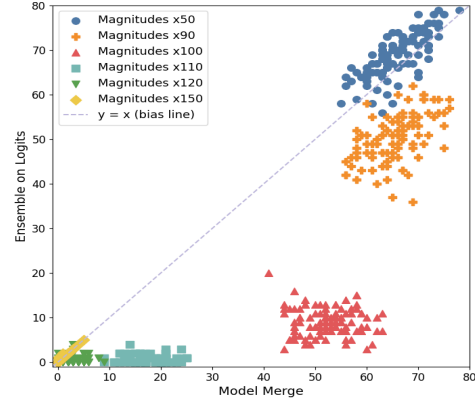


Figure 4. Scatter plot comparing the classification accuracies of model merge (uniform soup) and model ensemble (logits ensemble) over different weights magnitudes with VGG19 model on Cifar100. The values on the X and Y axis represent the accuracies. The experimental analysis is in Sec. 6.3.

In this section, we will examine how the weight-merging behaves against magnifying the candidate model weights by different magnitude factors. This helps us understand how robust model-merging works.

5.1. Analysis of Weight Magnitude After Averaging

We start from analyzing the effect of averaging the weights of two independent matrices, denoted as \mathbf{W}_1 and \mathbf{W}_2 , on their respective magnitudes. We define the maximum entry of both matrices as $M = \max(\mathbf{W}_1, \mathbf{W}_2) = \max_{i,j}(|(\mathbf{W}_1)_{i,j}|, |(\mathbf{W}_2)_{i,j}|)$. When we compute the averaged weights, we obtain:

$$\overline{\mathbf{W}} = \frac{\mathbf{W}_1 + \mathbf{W}_2}{2}. \quad (9)$$

We seek to understand the relationship between the max entry of the averaged weights $\overline{\mathbf{W}}$ and M .

Mathematical Justification. Using the triangle inequality [30], we establish:

$$\|\overline{\mathbf{W}}\| = \left\| \frac{\mathbf{W}_1 + \mathbf{W}_2}{2} \right\| \leq \frac{\|\mathbf{W}_1\| + \|\mathbf{W}_2\|}{2}, \quad (10)$$

where $\|\cdot\|$ denotes a matrix entry-wise max norm operator. Applying the property of maximum values, we have:

$$\frac{\|\mathbf{W}_1\| + \|\mathbf{W}_2\|}{2} \leq \max(\mathbf{W}_1, \mathbf{W}_2) = M. \quad (11)$$

Thus, it follows that $\|\bar{\mathbf{W}}\| \leq M$ combining with Eq. 10. It confirms that averaging the weights results in a new weight whose entry's upper bound is equal to the maximum entry of the original weights. Thus, the operation of averaging the weights \mathbf{W}_1 and \mathbf{W}_2 typically results in a reduction of the maximum weight magnitude. This conclusion also extends to complex deep neural networks.

5.2. Weight Variance Reduces while Averaging

We denote the means and variances of \mathbf{W}_1 and \mathbf{W}_2 as $\mathbb{E}(\mathbf{W}_1) = \mu_1$, $\text{Var}(\mathbf{W}_1) = \sigma_1^2$ and $\mathbb{E}(\mathbf{W}_2) = \mu_2$, $\text{Var}(\mathbf{W}_2) = \sigma_2^2$. Our goal is to compute the variance of $\bar{\mathbf{W}}$ and compare it to the variances of \mathbf{W}_1 and \mathbf{W}_2 . The expectation of the averaged weights $\bar{\mathbf{W}}$ is given by:

$$\mathbb{E}(\bar{\mathbf{W}}) = \mathbb{E}\left(\frac{\mathbf{W}_1 + \mathbf{W}_2}{2}\right) = \frac{\mathbb{E}(\mathbf{W}_1) + \mathbb{E}(\mathbf{W}_2)}{2} = \frac{\mu_1 + \mu_2}{2} \quad (12)$$

For the variance of $\bar{\mathbf{W}}$, we have:

$$\begin{aligned} \text{Var}(\bar{\mathbf{W}}) &= \text{Var}\left(\frac{\mathbf{W}_1 + \mathbf{W}_2}{2}\right) \\ &= \frac{1}{4} [\text{Var}(\mathbf{W}_1) + \text{Var}(\mathbf{W}_2)] = \frac{1}{4}(\sigma_1^2 + \sigma_2^2) \end{aligned} \quad (13)$$

Mathematical Justification. We now compare the variance of $\bar{\mathbf{W}}$ to the variances of \mathbf{W}_1 and \mathbf{W}_2 . If $\sigma_1 = \sigma_2 = \sigma$, then $\text{Var}(\bar{\mathbf{W}}) = \frac{1}{2}\sigma^2$. This shows that, when the variances of the two models are the same, the variance is reduced by a factor of two. More generally, we have:

$$\frac{1}{4}(\sigma_1^2 + \sigma_2^2) \leq \max(\sigma_1^2, \sigma_2^2) \quad (14)$$

Thus, the variance of the averaged model $\bar{\mathbf{W}}$ is always less than or equal to the larger member between σ_1^2 and σ_2^2 .

5.3. How Weight Magnitudes and Variance Effects Model Outputs

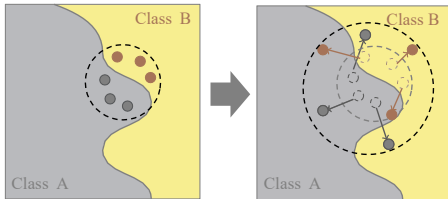


Figure 5. An illustration showing the magnitudes and variances of model outputs increasing over the increment of weights' magnitudes and variances, making the prediction no longer fall into the correct side of the decision boundary.

We have the following property 1 and theorem 1 to build the connections between model weights' magnitudes/variances and outputs' magnitudes/variances, following [34]:

Property 1: Let $f_\theta(x)$ be a fully-connected neural network, where θ is the parameters. Assume the activation function ϕ is Lipschitz continuous with constant L , and the weight matrices $\mathbf{W}^{(m)}$ are random matrices with independent and identically distributed (i.i.d.) sub-Gaussian entries. Then, for any input \mathbf{x} , the output at the m -th layer, $\mathbf{y}^{(m)}$, satisfies the following upper bound:

$$\|\mathbf{y}^{(m)}\|_2 \leq (L\lambda)^m \|\mathbf{x}\|_2, \text{ for } \forall \tau > 0 \quad (15)$$

with a probability of at least $(1 - 2e^{-\tau^2})^m$, where (m) indexes the neural network layer, with m representing the exponential operation, and $\lambda = \sqrt{N} + C_s K_s^2(\sqrt{N} + \tau)$, with N being the maximum number of neurons across all layers, C_s representing a constant, and $K_s = \max \|\mathbf{W}^{(m)}\|_2$. This property shows that the output norm can grow exponentially with the number of layers m , controlled by the Lipschitz constant of the activation function and bounded by the max entry value of weight matrices.

Theorem 1: Assume the weights in each layer are i.i.d. sub-Gaussian random variables with variance σ_w^2 , and the biases are with variance σ_b^2 . Also, let the activation function ϕ be Lipschitz continuous with constant L . Then, the variance of the output of the final layer, represented by $\mathbb{V}(f_\theta(x))$, can be bounded by:

$$\begin{aligned} \mathbb{V}(f_\theta(x)) &\leq \|\mathbf{x}\|_2^2 (L^2 N)^m \prod_{m=1}^{M_l} (\sigma_w^{(m)})^2 + L^2 N (\sigma_b^{(M_l)})^2 + \\ &L^2 \sum_{m=1}^{M-1} \left\{ N (\sigma_b^{(m)})^2 \prod_{l=m+1}^M \left[L^2 N (\sigma_w^{(l)})^2 \right] \right\}, \end{aligned} \quad (16)$$

where M_l denotes the maximum number of layers, and L represents the Lipschitz constant. This inequality shows that the output variance grows with the depth of the network, as well as impacted by the variances of the weights / bias.

Property 1 and Theorem 1 show that the increment of model weights' magnitudes/variances will also magnify outputs' magnitudes/variances. As shown in Fig. 5, consider a neural network with input \mathbf{x} and output \mathbf{y} , where weights are denoted as \mathbf{W} . When model weights have large magnitudes and high variance, predictions become unreliable. This issue can arise from several factors, including task specificity, lack of regularization or improper weight initialization. Together, these factors can drive the weights to unstable values, reducing the model's ability to generalize effectively. On the other hand, when $\mathbf{W} \rightarrow 0$, the output \mathbf{y} will tend to a fixed point determined predominantly by the network's bias terms, becoming largely independent of the input \mathbf{x} . Hence, if the magnitude of \mathbf{W} is small, but not identically zero, then the range of outputs for \mathbf{y} will be constrained. This reduces the sensitivity of \mathbf{y} to the changes of \mathbf{x} , effectively shrinking the output space. In this case, model-merging acts similar to the L1 or L2 regularization. Such behavior can enhance the robustness of the model, as smaller weight magnitudes reduce the model's response to minor perturbations in input \mathbf{x} . But this comes with a trade-off: the expressive capacity of models may diminish as well, potentially leading to compromised performance on complex tasks.

Proposal 3: As the aforementioned analyses and experimental study in Sec. 6.3, model-merging is more robust to the changes in weights’ magnitudes/variances than model ensemble, by bringing down the maximum magnitudes/variances of individual models before merging. This is because, generally, the small magnitudes of weights enhances robustness by minimizing the network’s sensitivity towards input variations, but somehow reduces the expressiveness from ensembling all models. From this perspective, model-merging acts similarly as regularization. This balance between robustness and expressiveness is crucial and should be carefully considered based on the specific task requirements. For certain tasks where noise resilience is more valuable than fine-grained feature sensitivity, lower weight magnitudes can improve performance.

6. Experiments

The experimental settings and details can be found in the supplementary materials.

6.1. The Patterns Contained in Model Weights

As shown in Fig. 1(a,b), the visualization of the linear classifier on Cifar100 explicitly shows the patterns per classifier learned, which are strongly correlated with the average of images per class. The patterns learned per class acts as a fused representative image. Interestingly, if we merge the weights of the first 5 classes with the last 5 classes in Fig. 1, it gives us the results of Fig. 2. As mentioned, the weight-averaged model-merging acts as a Mixup operation, which is a linear combination of different matrices, in the weight space. For instance, when the “bicycle” weight matrix is combined with the “bottle” weight matrix, we can see the wheels of bikes combined with a vertical bottle. We can also observe that, after merging, each element within the combined template noticeably fades. This phenomenon can also explain the limitation of expressiveness of the merged model as described in Sec. 4.

Fig. 6 visualizes the image average per class and its corresponding weight for Tiny ImageNet classes. For instance, “goldfish” shows a reddish center in the averaged images and also shows a reddish center in the classifier weights; similarly, we can observe the eyes and nose of “koala”; for pretzel, we can see the shape of the cracker from its weight visualization. However, they are not as clear as for Cifar100. This may be due to the relatively large dataset size, as the average of all images in a class itself is also vaguer. This compromised clarity can also be caused by the limited expressiveness of single linear classifiers and there are more complicated patterns present in Tiny ImageNet than Cifar100. Besides the linear classifier visualization, we also conduct common deep learning models with nonlinear weights visualization by viewing the first layer of convolutional kernels (7×7 in size) from the ResNet50 model [9] in Fig. 7 (VGG model weight visualization can be found in the supplementary materials). We can see the patterns of texture and edges for the basic level geometric feature detection is similar to the Haar features described in Sec. 3.1.

The visualizations for all classes within Cifar100 and Tiny ImageNet are put in the supplementary materials.

6.2. Weights vs. Features Averaging

6.2.1. Observations over Different Models

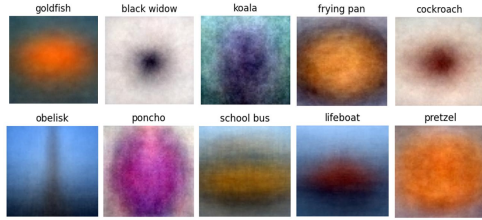
As shown in Fig. 3 for the merging of 10 models (the experiments for merging from 2 to 7 models are in the supplementary materials). For abbreviations, “Perf Ave” denotes the average performance of individual models; “deit_tiny” and “vit_tiny” denote deit_tiny_patch16_224 and vit_tiny_patch16_224 models, respectively. Different models show different merging/ensembling performances, but model ensemble on logits generally performs the best across different tested architectures [5, 9, 10, 24, 26, 29]. However, uniform soups perform the worst. We can also discover that greedy soups generally perform better than uniform soups due to their mechanism to greedily select the best performing model to merge. In fact, it guarantees that reasonably promising results can be achieved by only incorporating the first model (if the later-on merged model performance is not ideal). The greedy ensemble on both logits and features produces results that are comparable to greedy soups.

In general, adding more models into the merging process leads to better performance for all methods, including model-merging and ensembling. Interestingly, the ViT model, including 3 ViT-based architectures in the experiments, shows large gaps between uniformly averaging and logits ensembling, where such gaps suffer larger increases by adding more models into. This happens may be caused by the architectural differences between convolutional neural networks and Vision Transformers (ViTs). CNNs are more adapted to the learning of local patterns within different scales of images, making it ideal for merging. On the contrary, ViTs have global attention mechanisms, where the templates represent attention and correlations between tokens, making them sensitive for small changes. ViT models also show similar deterioration on other data (as shown by the DeiT on TinyImageNet and it can be found in the supplementary materials).

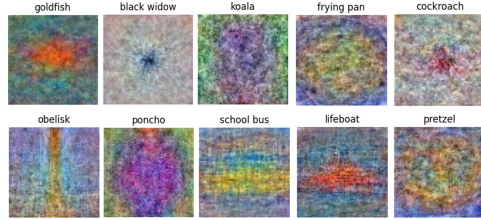
We also visualize the gaps between Logits Ensemble and Uniform Soups Across Different Configurations (excluding ViT models as the gaps are too large, so in different scales) in Fig. 8(a). We can see that the more models in the merging process, the larger the gap between logits ensemble and uniform soups. The gaps are different according to different models, but generally, there is a downtrend when models contain more layers (e.g., ResNet18 to ResNet152, DenseNet121 to DenseNet201, VGG11 to VGG19 without BatchNorm). This may be caused by the performance saturation when more layers are included, as the model will be empowered with stronger fitting abilities. But batch normalization can break this trend. We have also examined the gaps between logits ensemble and greedy soups in the supplementary materials, showing that greedy soups can alleviate this marginal effect.

6.2.2. Observations over Different Datasets

For the dataset-wise examination, we perform model-merging and ensembling on 7 prevalent datasets with different data sizes (TinyImageNet and ChestXRay are relatively large, and both with more than 100,000 images in the datasets). From Tab. 1, we can observe that the ensembling still generally performs better than merging. The models on different datasets have different performances due to the dataset characteristics. Similarly to the model-wise comparison, with more models in the merging process (2 to 7 models merging results are in the supplementary materials), the better



(a) Average of all images for each class.



(b) Linear classifiers visualization.

Figure 6. Average of all images for each class and linear classifiers visualization for each class in Tiny ImageNet [15] dataset.

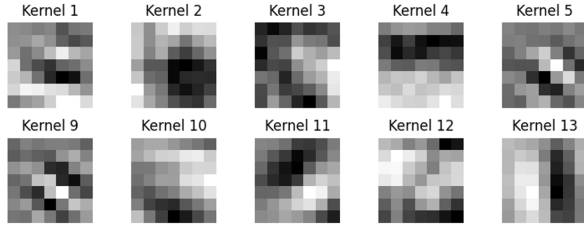


Figure 7. The examples of the first layer weights visualization of Resnet50 with nonlinearity inside the model.

Table 1. Performance Comparison for VGG19 with 10 Models Across Different Datasets. We adopt averaged AUROC (Area Under Curve of Receiver Operating Characteristic) as the evaluation metric (normalized into 0 to 100 for better representation with other datasets) for the ChestXRay [18, 33] dataset; while accuracy (0% to 100%) for the rest of datasets.

Datasets	Perf Ave	Uni Soups	Grd Soups	Ens Lgt	Ens Fts	Grd Ens	Lgt Ens	Fts Ens
Cifar10	92.37	92.90	92.62	93.91	93.81	92.63	92.62	92.62
Cifar100	70.34	69.63	70.25	75.36	74.96	70.39	70.32	70.32
PathMNIST	90.04	32.42	88.48	92.95	75.17	88.59	88.34	88.34
DermaMNIST	74.17	68.18	74.16	75.76	69.73	73.92	73.17	73.17
Celeba	92.91	53.19	93.06	93.44	93.47	93.02	93.04	93.04
TinyImageNet	59.90	62.31	61.95	63.28	63.53	63.53	63.58	63.58
ChestXRay	80.66	79.29	80.43	81.77	81.07	80.43	80.43	80.43

the performance for both merging and ensembling. The ensembling is more stable than merging in terms of the best and worst performance on different datasets. For example, on the PathMNIST [39, 40], uniform soup does not work very well (32.42% accuracy, which largely behind model ensemble methods) compared to its performance on the Cifar10/Cifar100 or Tiny ImageNet datasets. A similar situation shows on Celeba [17]: the uniformly average model only achieves 53.19%. Nevertheless, the greedy soup models can mitigate this problem (88.48% on PathMNIST and 93.06 on Celeba) as they can ensure a decent result by only considering the first model. These results may be caused by the contradictions between model weights.

6.2.3. Merging Models trained over different Tasks

We also explore model-merging between different well-trained models on different tasks, as shown in Tab. 2. Model 1 is a VGG19 model trained on the Cifar100 with the classification accuracy of 70.37%, while Model 2 denotes the VGG19 model trained on different datasets, but evaluated on Cifar100 after merging/ensembling.

Table 2. Performance Comparison for Task Merging Across Different Datasets with Various Model Averaging Methods. Model 1 is a VGG19 model trained on the Cifar100 with the classification accuracy of 70.37%, while Model 2 denotes the VGG19 model trained on different datasets, but evaluated on Cifar100 after merging/ensembling. E.g. Model 2 trained on Cifar10 receives 5.84% accuracy on Cifar100 dataset.

Datasets	Data Size	Model2	Uniform Soups	Ens Lgt	Ens Features
Cifar10	60,000	5.84	49.63	69.93	69.93
PathMNIST	107,180	1.29	24.25	69.88	70.00
DermaMNIST	10,015	5.77	60.37	69.06	69.36
Celeba	202,599	1.03	49.33	69.48	69.61
TinyImageNet	100,000	18.16	61.02	58.40	58.52
ChestXRay	112,120	15.18	61.38	68.18	68.33

ing/ensembling. Generally, uniform souping within Tiny ImageNet, where Model 2 was trained on, has the highest accuracy of 61.02% that is better than the ensemble on logits (58.40% accuracy). It may be because the Tiny ImageNet dataset is a general and relatively large dataset, forcing Model 2 to learn a diverse set of features. Interestingly, Cifar10 should be a similar one to Cifar100, but the souping result does not outperform the model ensembling. Maybe because it is too small. In contrast, the ChestXRay dataset should be very different from Cifar100, but it shows a reasonably decent improvement with souping compared to Model 2 along. It illustrates that the dataset size also matters. The souping performance on Celeba (Model 2 is trained on) is not good, may be caused by the Celeba dataset only containing human faces that are very different from Cifar100 (Model 1 is trained on).

6.3. Model Predictions and Weight Magnitudes

The increment in weight magnitudes also increases the variance of weights. As shown in Fig. 4 (each accuracy point of merging and ensembling is obtained from the same batch of data), when the magnitude factor is not too large ($\times 50$), we can roughly see a positive linear correlation between model-merging and model ensembling performance. More points are above the diagonal bias line, meaning the ensembling is slightly better. However, this trend is broken when larger magnitude factors are introduced ($\geq \times 90$). When $\times 90$ is used as the magnitude factor, we can still observe the positive correlation between the two types of methods, but all points are below the bias line. With larger magnitude factors (above $\geq \times 100$), the positive correlations disappear. It clearly shows that the model-merging can have better robustness against

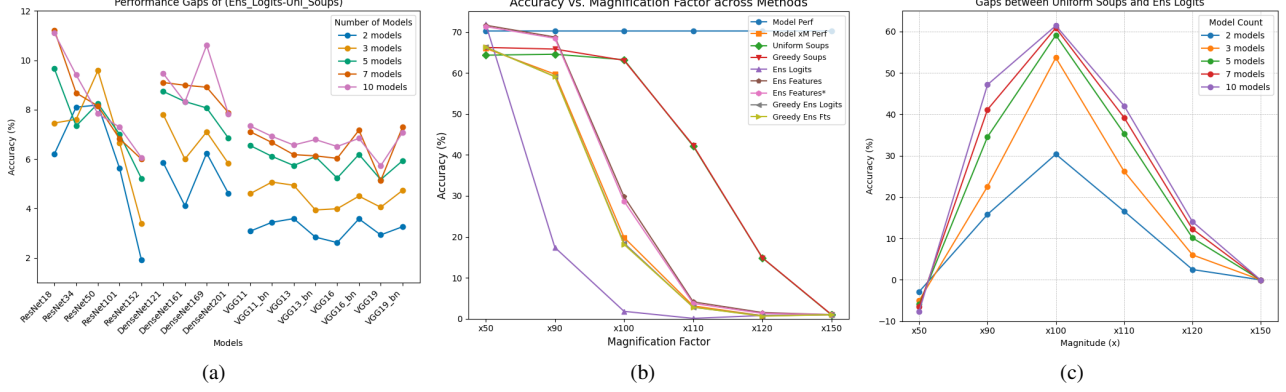


Figure 8. (a) For Sec. 6.2, performance Gaps between Logits Ensemble and Uniform Soups Across Different Configurations (excluded the ViT models as the scales are too different) on Cifar100. (b) For Sec. 6.3, accuracy vs. Magnification Factor across Methods with 10 models on Cifar100 dataset. (c) For Sec. 6.3, Uniform soup - Logits Ensemble Accuracy vs. Magnification Factor in terms of different model numbers on Cifar100 dataset.

weight magnitudes and variance changes with large magnitude factors.

Moreover, we visualize 10 models (merging of 2 to 7 models can be found in the supplementary materials) merging and ensembling towards different magnitude factors, as shown in Fig. 8b. In the figure, “Model Perf” denotes the average of individual model performance without magnifying the weights (that is why it is a constant value), and “Model $\times M$ Perf” represents the model with different magnification. From the trends in the figures, we can observe the merged models are more robust than ensembled ones (with the factor grows, the line denoting ensembling goes down quickly), including ensemble on logits and features. But interestingly, feature ensembling is more robust than logits ensembling across different configurations. Feature ensembling can even outperform model-merging when weight magnification is not large (e.g., $\times 50$). This shows the feature ensembling can have some resistance towards the change of weight magnitudes. The “Ens Features” performs ensemble on multiple model features, while merging all last fully connected (FC) layers to get rid of the influence of FC layer. In order to mitigate the impact of the merged FC layer, we introduce a variant of the model, “Ens Features*”, by directly adopting the FC layer from the 1st model. We can observe the “Ens Features” and “Ens Features*” models perform similarly. It shows the low sensitivity of the merging of last layers.

We further visualize the gaps between model-merging and ensembling in Fig. 8c. When more models are taken into account, the gaps become larger, but there is a peak point for the gap ($\times 100$ is the peak for Cifar100). The experiments of merging/ensembling 2 to 10 models with different magnitude factors, as well as on different datasets and the gaps between merging and ensembling, are shown in the supplementary materials. A similar phenomenon is shown on different datasets, but with different peaks. Moreover, we conduct the weight magnitude experiment on a relatively large dataset, Tiny ImageNet, in Tab. 3. From the table, we can observe that model-merging can still mitigate the weight magnifying problem to a certain extent. It can also outperform logit ensembling, and cannot outperform feature ensembling. But generally it cannot work very well as on Cifar100. It may be caused by the complex-

ity of the Tiny ImageNet and as we discussed in the Sec. 5.3, the model-merging can work to some extent as it can act similarly as regularization. It can mitigate the weight magnitude increment issues, but with the cost of losing model expressiveness.

Table 3. Model-merging to address the weight magnitude issue for VGG19 with different model numbers on Tiny ImageNet dataset with the magnitude factor $\times 100$. This approach works for smaller data (Cifar10/Cifar100) as it has a regularization effect. However, it does not work for larger datasets such as Tiny ImageNet, because it sacrifices the expressiveness of the models.

Model #	Perf Ave	$\times M$ Perf	Uni Soups	Grd Soups	Ens Lgt	Ens Fts	Ens Fts*	Grd Ens	Lgt Ens	Grd Ens	Fts Ens
2 models	59.87	5.60	6.70	6.99	1.59	6.94	6.45	1.52	6.96		
3 models	59.85	5.44	7.15	7.05	0.78	7.38	6.78	0.78	7.21		
5 models	59.89	5.07	6.68	6.83	0.30	6.95	6.46	0.35	7.21		
7 models	59.90	4.80	6.77	6.80	0.24	6.73	6.26	0.21	6.74		
10 models	59.90	4.81	6.86	6.92	0.13	6.92	6.22	0.11	6.95		

7. Conclusion

In this paper, we thoroughly examined the weight-averaged model-merging approach through the lens of template matching by visualizing weight patterns across various datasets. Our comparison of weight and feature averaging within ensembling and merging methods revealed notable differences in their effects on different architectures and datasets, offering insights into when and why each approach is beneficial. Furthermore, we demonstrate that model-merging techniques tend to yield more stable predictions than model ensembles, especially when subjected to variations in parameter magnitudes, thus enhancing robustness and generalization. These findings clarify the interpretability and key aspects of model-merging, providing a deeper understanding of its application across diverse contexts. We anticipate that these insights will stimulate further research into model-merging strategies and support the development of more interpretable and robust model-averaging methodologies.

References

- [1] Samuel K Ainsworth, Jonathan Hayase, and Siddhartha Srinivasa. Git re-basin: Merging models modulo permutation symmetries. *arXiv preprint arXiv:2209.04836*, 2022. 2
- [2] Francesco Croce, Sylvestre-Alvise Rebuffi, Evan Shelhamer, and Sven Gowal. Seasoning model soups for robustness to adversarial and natural distribution shifts. In *Proceedings of the IEEE/CVF Conference on Computer Vision and Pattern Recognition*, pages 12313–12323, 2023. 1
- [3] Nico Daheim, Thomas Möllenhoff, Edoardo Maria Ponti, Iryna Gurevych, and Mohammad Emtiyaz Khan. Model merging by uncertainty-based gradient matching. *arXiv preprint arXiv:2310.12808*, 2023. 1
- [4] Jasper Dekoninck, Marc Fischer, Luca Beurer-Kellner, and Martin Vechev. Controlled text generation via language model arithmetic. *arXiv preprint arXiv:2311.14479*, 2023. 3
- [5] Alexey Dosovitskiy. An image is worth 16x16 words: Transformers for image recognition at scale. *arXiv preprint arXiv:2010.11929*, 2020. 6, 1
- [6] Rahim Entezari, Hanie Sedghi, Olga Saukh, and Behnam Neyshabur. The role of permutation invariance in linear mode connectivity of neural networks. *arXiv preprint arXiv:2110.06296*, 2021. 2
- [7] Yoav Freund, Robert Schapire, and Naoki Abe. A short introduction to boosting. *Journal-Japanese Society For Artificial Intelligence*, 14(771-780):1612, 1999. 2
- [8] Timur Garipov, Pavel Izmailov, Dmitrii Podoprikin, Dmitry P Vetrov, and Andrew G Wilson. Loss surfaces, mode connectivity, and fast ensembling of dnns. *Advances in neural information processing systems*, 31, 2018. 2
- [9] Kaiming He, Xiangyu Zhang, Shaoqing Ren, and Jian Sun. Deep residual learning for image recognition. In *Proceedings of the IEEE conference on computer vision and pattern recognition*, pages 770–778, 2016. 6, 1
- [10] Gao Huang, Zhuang Liu, Laurens Van Der Maaten, and Kilian Q Weinberger. Densely connected convolutional networks. In *Proceedings of the IEEE conference on computer vision and pattern recognition*, pages 4700–4708, 2017. 6, 1
- [11] Gabriel Ilharco, Marco Tulio Ribeiro, Mitchell Wortsman, Suchin Gururangan, Ludwig Schmidt, Hannaneh Hajishirzi, and Ali Farhadi. Editing models with task arithmetic. *arXiv preprint arXiv:2212.04089*, 2022. 3
- [12] Keller Jordan, Hanie Sedghi, Olga Saukh, Rahim Entezari, and Behnam Neyshabur. Repair: Renormalizing permuted activations for interpolation repair. *arXiv preprint arXiv:2211.08403*, 2022. 2
- [13] Simran Khanuja, Melvin Johnson, and Partha Talukdar. Mergedistill: Merging pre-trained language models using distillation. *arXiv preprint arXiv:2106.02834*, 2021. 1
- [14] Alex Krizhevsky. Learning multiple layers of features from tiny images. Technical report, University of Toronto, 2009. 2, 1
- [15] Ya Le and Xuan Yang. Tiny imagenet visual recognition challenge. *CS 231N*, 7(7):3, 2015. 7, 1
- [16] Weishi Li, Yong Peng, Miao Zhang, Liang Ding, Han Hu, and Li Shen. Deep model fusion: A survey. *arXiv preprint arXiv:2309.15698*, 2023. 1
- [17] Ziwei Liu, Ping Luo, Xiaogang Wang, and Xiaoou Tang. Deep learning face attributes in the wild. In *Proceedings of International Conference on Computer Vision (ICCV)*, 2015. 7, 1
- [18] Congbo Ma, Hu Wang, and Steven CH Hoi. Multi-label thoracic disease image classification with cross-attention networks. In *Medical Image Computing and Computer Assisted Intervention–MICCAI 2019: 22nd International Conference, Shenzhen, China, October 13–17, 2019, Proceedings, Part VI 22*, pages 730–738. Springer, 2019. 7, 1
- [19] Michael S Matena and Colin A Raffel. Merging models with fisher-weighted averaging. *Advances in Neural Information Processing Systems*, 35:17703–17716, 2022. 2
- [20] Tomas Mikolov. Efficient estimation of word representations in vector space. *arXiv preprint arXiv:1301.3781*, 3781, 2013. 3
- [21] Aviv Navon, Aviv Shamsian, Ethan Fetaya, Gal Chechik, Nadav Dym, and Haggai Maron. Equivariant deep weight space alignment. *arXiv preprint arXiv:2310.13397*, 2023. 1
- [22] Alexandre Rame, Guillaume Couairon, Corentin Dancette, Jean-Baptiste Gaya, Mustafa Shukor, Laure Soulier, and Matthieu Cord. Rewarded soups: towards pareto-optimal alignment by interpolating weights fine-tuned on diverse rewards. *Advances in Neural Information Processing Systems*, 36, 2024. 1
- [23] Santosh Sanjeev, Nuren Zhaksylyk, Ibrahim Almakky, Anees Ur Rehman Hashmi, Mohammad Areeb Qazi, and Mohammad Yaqub. Fissionfusion: fast geometric generation and hierarchical souping for medical image analysis. In *International Conference on Medical Image Computing and Computer-Assisted Intervention*, pages 131–141. Springer, 2024. 1
- [24] Karen Simonyan. Very deep convolutional networks for large-scale image recognition. *arXiv preprint arXiv:1409.1556*, 2014. 6, 1
- [25] Sidak Pal Singh and Martin Jaggi. Model fusion via optimal transport. *Advances in Neural Information Processing Systems*, 33:22045–22055, 2020. 1
- [26] Andreas Steiner, Alexander Kolesnikov, Xiaohua Zhai, Ross Wightman, Jakob Uszkoreit, and Lucas Beyer. How to train your vit? data, augmentation, and regularization in vision transformers. *arXiv preprint arXiv:2106.10270*, 2021. 6, 1
- [27] George Stoica, Daniel Bolya, Jakob Bjorner, Pratik Ramesh, Taylor Hearn, and Judy Hoffman. Zipit! merging models from different tasks without training. *arXiv preprint arXiv:2305.03053*, 2023. 2
- [28] Yi-Lin Sung, Linjie Li, Kevin Lin, Zhe Gan, Mohit Bansal, and Lijuan Wang. An empirical study of multimodal model merging. *arXiv preprint arXiv:2304.14933*, 2023. 1
- [29] Hugo Touvron, Matthieu Cord, Matthijs Douze, Francisco Massa, Alexandre Sablayrolles, and Hervé Jégou. Training data-efficient image transformers & distillation through attention. In *International conference on machine learning*, pages 10347–10357. PMLR, 2021. 6, 1

- [30] Amos Tversky and Itamar Gati. Similarity, separability, and the triangle inequality. *Psychological review*, 89(2):123, 1982. [4](#)
- [31] Paul Viola and Michael Jones. Rapid object detection using a boosted cascade of simple features. In *Proceedings of the 2001 IEEE computer society conference on computer vision and pattern recognition. CVPR 2001*, pages I–I. Ieee, 2001. [2](#)
- [32] Hongyi Wang, Mikhail Yurochkin, Yuekai Sun, Dimitris Papailiopoulos, and Yasaman Khazaeni. Federated learning with matched averaging. *arXiv preprint arXiv:2002.06440*, 2020. [1](#)
- [33] Xiaosong Wang, Yifan Peng, Le Lu, Zhiyong Lu, Mohammadhadi Bagheri, and Ronald M Summers. Chestx-ray8: Hospital-scale chest x-ray database and benchmarks on weakly-supervised classification and localization of common thorax diseases. In *Proceedings of the IEEE conference on computer vision and pattern recognition*, pages 2097–2106, 2017. [7](#), [1](#)
- [34] Zihan Wang, Zhongkui Ma, Xinguo Feng, Ruoxi Sun, Hu Wang, Minhui Xue, and Guangdong Bai. Corelocker: Neuron-level usage control. In *2024 IEEE Symposium on Security and Privacy (SP)*, pages 222–222. IEEE Computer Society, 2024. [5](#), [1](#)
- [35] Mitchell Wortsman, Gabriel Ilharco, Samir Ya Gadre, Rebecca Roelofs, Raphael Gontijo-Lopes, Ari S Morcos, Hongseok Namkoong, Ali Farhadi, Yair Carmon, Simon Kornblith, et al. Model soups: averaging weights of multiple fine-tuned models improves accuracy without increasing inference time. In *International conference on machine learning*, pages 23965–23998. PMLR, 2022. [1](#), [2](#)
- [36] Prateek Yadav, Derek Tam, Leshem Choshen, Colin A Raffel, and Mohit Bansal. Ties-merging: Resolving interference when merging models. *Advances in Neural Information Processing Systems*, 36, 2024. [2](#)
- [37] Enneng Yang, Zhenyi Wang, Li Shen, Shiwei Liu, Guibing Guo, Xingwei Wang, and Dacheng Tao. Adamerging: Adaptive model merging for multi-task learning. *arXiv preprint arXiv:2310.02575*, 2023. [1](#)
- [38] Enneng Yang, Li Shen, Guibing Guo, Xingwei Wang, Xiaochun Cao, Jie Zhang, and Dacheng Tao. Model merging in llms, mllms, and beyond: Methods, theories, applications and opportunities. *arXiv preprint arXiv:2408.07666*, 2024. [1](#)
- [39] Jiancheng Yang, Rui Shi, and Bingbing Ni. Medmnist classification decathlon: A lightweight automl benchmark for medical image analysis. In *IEEE 18th International Symposium on Biomedical Imaging (ISBI)*, pages 191–195, 2021. [7](#), [1](#)
- [40] Jiancheng Yang, Rui Shi, Donglai Wei, Zequan Liu, Lin Zhao, Bilian Ke, Hanspeter Pfister, and Bingbing Ni. Medmnist v2-a large-scale lightweight benchmark for 2d and 3d biomedical image classification. *Scientific Data*, 10(1):41, 2023. [7](#), [1](#)
- [41] Le Yu, Bowen Yu, Haiyang Yu, Fei Huang, and Yongbin Li. Language models are super mario: Absorbing abilities from homologous models as a free lunch. In *Forty-first International Conference on Machine Learning*, 2024. [2](#)
- [42] Hongyi Zhang. mixup: Beyond empirical risk minimization. *arXiv preprint arXiv:1710.09412*, 2017. [3](#)
- [43] Jinghan Zhang, Junteng Liu, Junxian He, et al. Composing parameter-efficient modules with arithmetic operation. *Advances in Neural Information Processing Systems*, 36: 12589–12610, 2023. [3](#)
- [44] Jinghuai Zhang, Jianfeng Chi, Zheng Li, Kunlin Cai, Yang Zhang, and Yuan Tian. Badmerging: Backdoor attacks against model merging. *arXiv preprint arXiv:2408.07362*, 2024. [1](#)
- [45] Yuyan Zhou, Liang Song, Bingning Wang, and Weipeng Chen. Metagpt: Merging large language models using model exclusive task arithmetic. *arXiv preprint arXiv:2406.11385*, 2024. [1](#)
- [46] Zhanpeng Zhou, Zijun Chen, Yilan Chen, Bo Zhang, and Junchi Yan. On the emergence of cross-task linearity in pretraining-finetuning paradigm. In *Forty-first International Conference on Machine Learning (ICML 2024)*. [3](#)

Rethinking Weight-Averaged Model-merging

Supplementary Material

8. Experimental Settings

For the experimental settings of **model weight patterns**. We train one single linear layer on both Cifar100 [14] and Tiny ImageNet [15] datasets with momentum SGD as the optimizer. The initial learning rate is set to 0.01 and decreases every 20 epochs by 0.1. While visualization, the weights are wrapped back to the image size as described in the main paper (i.e. $100 \times 3 \times 32 \times 32$ for Cifar100).

In terms of **averaging on weights versus averaging on features**, we consider Uniform Soups and Greedy Soups [35] for weight-averaged model-merging, which is the focus of our paper. We design the experiments of this section from two different angles: model-wise examination and dataset-wise examination of the model-merging and model ensemble performances. For the models considered, we have ResNet [9] (ResNet18 to ResNet152), DenseNet [10] (DenseNet121 to DenseNet201), VGG [24] (VGG11 to VGG19, including with and without batch normalization), ViT [5, 26] and DeiT [29]. For the dataset-wise examination, we conduct experiments on Cifar10/Cifar100, PathMNIST/DermaMNIST [39, 40], Celeba [17], Tiny ImageNet and ChestXRay [18, 33]. The information of these datasets can be found in Tab. 4. Specially, ChestXRay-14 is a chest X-ray imaging dataset designed for multi-label classification. It consists of 112,120 frontal chest X-ray images from 30,805 unique patients. The dataset includes annotations for 14 different lung disease categories. We use the official dataset split for training and evaluation. We demonstrate the average Area Under the Receiver Operating Characteristic Curve (AUROC) across 14 labels as the model performance for ChestXRay.

For model ensembling, we consider to ensemble on model logits (before entering softmax or sigmoid) and ensemble on model features (before the final classification layer). Besides these two model ensembling techniques, whenever a model is considered to be merged into a greedy soup model, we also ensemble it with either we called the Greedy Ensemble Logits model (Grd Ens Lgt) or Greedy Ensemble Features model (Grd Ens Fts). In order to exclude the impact of adopting the last layer from any single model, the ‘‘Ens Features’’ model uses the merging of the last fully connected (FC) layers from all merged models for classification.

For the experiments of **model predictions and weight magnitudes**, we conduct experiments on Cifar10, Cifar100 and Tiny ImageNet datasets. To increase the magnitude and the variance of model weights, we magnify the model weights by a magnitude factor. Formally, when each element in a matrix A is scaled by a factor c , the variance of the resulting matrix elements increases proportionally to the square of this factor. For example, in the case where $c = 100$, the variance of the elements of matrix A becomes $100^2 \times \text{Var}(A) = 10,000 \times \text{Var}(A)$.

For all experiments in the paper, to keep fair comparisons, we adopt the official splits for each dataset. If they provide publicly available dataset with Python interface, we directly call the interface to import the data. Also, we uniformly train 10 models and

perform the model-merging and ensembling under exactly same conditions (learning rates, step strategies and optimizers, model numbers, etc).

9. Theoretical Proofs

For Eq. 14 in the paper, we aim to prove that:

$$\frac{1}{4}(\sigma_1^2 + \sigma_2^2) \leq \max(\sigma_1^2, \sigma_2^2)$$

Assume without loss of generality that $\sigma_1^2 \leq \sigma_2^2$ (the argument is symmetric if $\sigma_2^2 \leq \sigma_1^2$).

Given that $\max(\sigma_1^2, \sigma_2^2) = \sigma_2^2$, the inequality becomes:

$$\frac{1}{4}(\sigma_1^2 + \sigma_2^2) \leq \sigma_2^2$$

Now, observe the following:

$$\frac{1}{4}(\sigma_1^2 + \sigma_2^2) \leq \frac{1}{4}(2\sigma_2^2) = \frac{\sigma_2^2}{2}$$

Since $\frac{\sigma_2^2}{2} \leq \sigma_2^2$, we conclude that:

$$\frac{1}{4}(\sigma_1^2 + \sigma_2^2) \leq \sigma_2^2 = \max(\sigma_1^2, \sigma_2^2)$$

Thus, the inequality holds true.

For the Property 1 and Theorem 1, according to [34], we have:

Lemma 1: Given a fully-connected network, its weight matrix $\mathbf{W}^{(m)}$ satisfies, for any $\tau > 0$,

$$\|\mathbf{W}^{(m)}\|_2 \leq \sqrt{N} + C_s K_s^2 (\sqrt{N} + \tau),$$

with a probability of at least $1 - 2e^{-\tau^2}$, where C_s is a universal constant and $K_s = \max_i \|\mathbf{W}_i^{(m)}\|_2$.

For **Property 1**:

Proof. We denote $s_1(A)$ as the maximum singular value of A and set $\lambda = \sqrt{N} + C_s K_s^2 (\sqrt{N} + \tau)$ as the upper bound of the maximum singular value of all weight matrices by Lemma 1. By Lipschitz property of the activation function ϕ and $\|\mathbf{A}\mathbf{x}\| = s_1(A)\|\mathbf{x}\|$,

$$\begin{aligned} \|\mathbf{y}^{(m)}\|_2 &= \|\phi(\mathbf{W}^{(m)} \mathbf{y}_k^{(m-1)})\|_2 \\ &= \|\phi(\mathbf{W}^{(m)} \mathbf{y}_k^{(m-1)}) - \phi(0)\|_2 \\ &\leq L \|\mathbf{W}^{(m)} \mathbf{y}_k^{(m-1)} - 0\|_2 \\ &= L \|\mathbf{W}^{(m)} \mathbf{y}^{(m-1)}\|_2 \\ &= L s_1(\mathbf{W}^{(m)}) \|\mathbf{y}^{(m-1)}\|_2 \\ &\leq L \lambda \|\mathbf{y}^{(m-1)}\|_2 \\ &\leq (L \lambda)^2 \|\mathbf{y}^{(m-2)}\|_2 \\ &\dots \\ &\leq (L \lambda)^m \|\mathbf{x}\|_2. \end{aligned}$$

Table 4. The table shows dataset size, class number, and link for each of the dataset. In particular, ChestXRay dataset has 14 labels and each of them is a binary classification task.

Datasets	Sizes	Class #	Links
Cifar10	60,000	10	https://www.cs.toronto.edu/~kriz/cifar.html
Cifar100	60,000	100	https://www.cs.toronto.edu/~kriz/cifar.html
PathMNIST	107,180	9	https://medmnist.com/
DermaMNIST	10,015	7	https://medmnist.com/
CelebA	202,599	2	https://mmlab.ie.cuhk.edu.hk/projects/CelebA.html
TinyImageNet	100,000	200	https://huggingface.co/datasets/zh-plus/tiny-imagenet
ChestXRay	112,120	14×2	https://www.kaggle.com/paultimothymooney/chest-xray-pneumonia

Then we calculate the probability that this inequality holds by Lemma 1,

$$\begin{aligned}
& \mathbb{P}\left(\left\|\mathbf{y}^{(m)}\right\|_2 \leq (L\lambda)^m \|\mathbf{x}\|_2\right) \\
&= \prod_{k=1}^m \mathbb{P}\left(\left\|\mathbf{W}^{(k)} \mathbf{y}^{(k-1)}\right\|_2 \leq s_1(\mathbf{W}^{(k)}) \left\|\mathbf{y}^{(k-1)}\right\|_2\right) \\
&\geq (1 - 2e^{-\tau^2})^m.
\end{aligned}$$

□

For **Theorem 1**:

Proof. For the first hidden layer, we have a linear transformation for one neuron:

$$\mathbf{W}_i^{(1)} \mathbf{x} + b_i^{(1)}.$$

Given that all weights and biases are i.i.d, we get:

$$\begin{aligned}
\mathbb{V}(\mathbf{W}_i^{(1)} \mathbf{x} + b_i^{(1)}) &= \mathbb{V}\left(\sum_{j=1}^{N^{(1)}} \mathbf{W}_{i,j}^{(1)} x_j + b_i^{(1)}\right) \\
&= \mathbb{V}\left(\sum_{j=1}^{N^{(1)}} \mathbf{W}_{i,j}^{(1)} x_j\right) + \mathbb{V}(b_i^{(1)}) \\
&= \sum_{j=1}^{N^{(1)}} x_j^2 \mathbb{V}(\mathbf{W}_{i,j}^{(1)}) + \mathbb{V}(b_i^{(1)}) \\
&= (\sigma_w^{(1)})^2 \sum_{j=1}^{N^{(1)}} x_j^2 + (\sigma_b^{(1)})^2 \\
&= (\sigma_w^{(1)})^2 \|\mathbf{x}\|_2^2 + (\sigma_b^{(1)})^2.
\end{aligned}$$

By the Lipschitz property of the activation function, we have:

$$f_i^{(1)} = \phi(\mathbf{W}_i^{(1)} \mathbf{x} + b_i^{(1)}) \leq L(\mathbf{W}_i^{(1)} \mathbf{x} + b_i^{(1)}).$$

Then,

$$\begin{aligned}
\mathbb{V}(f_i^{(1)}) &\leq \mathbb{V}[L(\mathbf{W}_i^{(1)} \mathbf{x} + b_i^{(1)})] \\
&\leq L^2 \mathbb{V}(\mathbf{W}_i^{(1)} \mathbf{x} + b_i^{(1)}) \\
&\leq L^2 \left[(\sigma_w^{(1)})^2 \|\mathbf{x}\|_2^2 + (\sigma_b^{(1)})^2 \right].
\end{aligned}$$

Hence,

$$\begin{aligned}
\mathbb{V}(f^{(1)}) &= \sum_{j=1}^N \mathbb{V}(f_j^{(1)}) \\
&\leq L^2 N \left[(\sigma_w^{(1)})^2 \|\mathbf{x}\|_2^2 + (\sigma_b^{(1)})^2 \right].
\end{aligned}$$

Similarly, for other layers:

$$\mathbb{V}(f^{(m)}) \leq L^2 N^{(m-1)} \left[(\sigma_w^{(m)})^2 \|f^{(m-1)}\|_2^2 + (\sigma_b^{(m)})^2 \right].$$

This result follows by iteratively applying the inequalities, concluding the proof. □

10. More Visualization of Model Weight Patterns

Similar to the visualization in the main paper, we visualize the average of all images Fig. 9 and linear classifiers for all classes Fig. 10 within each class (all 100 classes) of Cifar100 dataset. We can clearly observe the strong correlation between the average of images per class and its learned weights.

We further visualize the linear classifiers after pair-wise merging between the first 50 classes and the last 50 classes in Cifar100 dataset as Fig. 11. We can see the combinations of two templates, e.g. “motorcycle+woman”.

More visualization of the convolutional kernels on Cifar100 within deep learning models, e.g. Fig. 12 for ResNet50 and Fig. 13 for VGG19. For ResNet50 kernel visualization, we can observe differences or similarities between each learned patterns. For instance, Kernel 5 and kernel 9 are similar in terms of textures and grayscale colors, which are responsible for detecting similar features and thus yield a similar activations (e.g. inner product) when interact with inputs; while Kernel 9 is very different with Kernel 45. The patterns inside ResNet50 is more human-friendly to be observed than VGG19, as ResNet50 models have larger kernel sizes.

In terms of Tiny ImageNet, we have Fig. 14 and Fig. 16 for the average of all images within 200 classes; also, Fig. 15 and Fig. 17 for the linear classifier visualization of all 200 classes in the dataset. We can observe the correlations between averaged images and the learned patterns show a similar phenomenon.

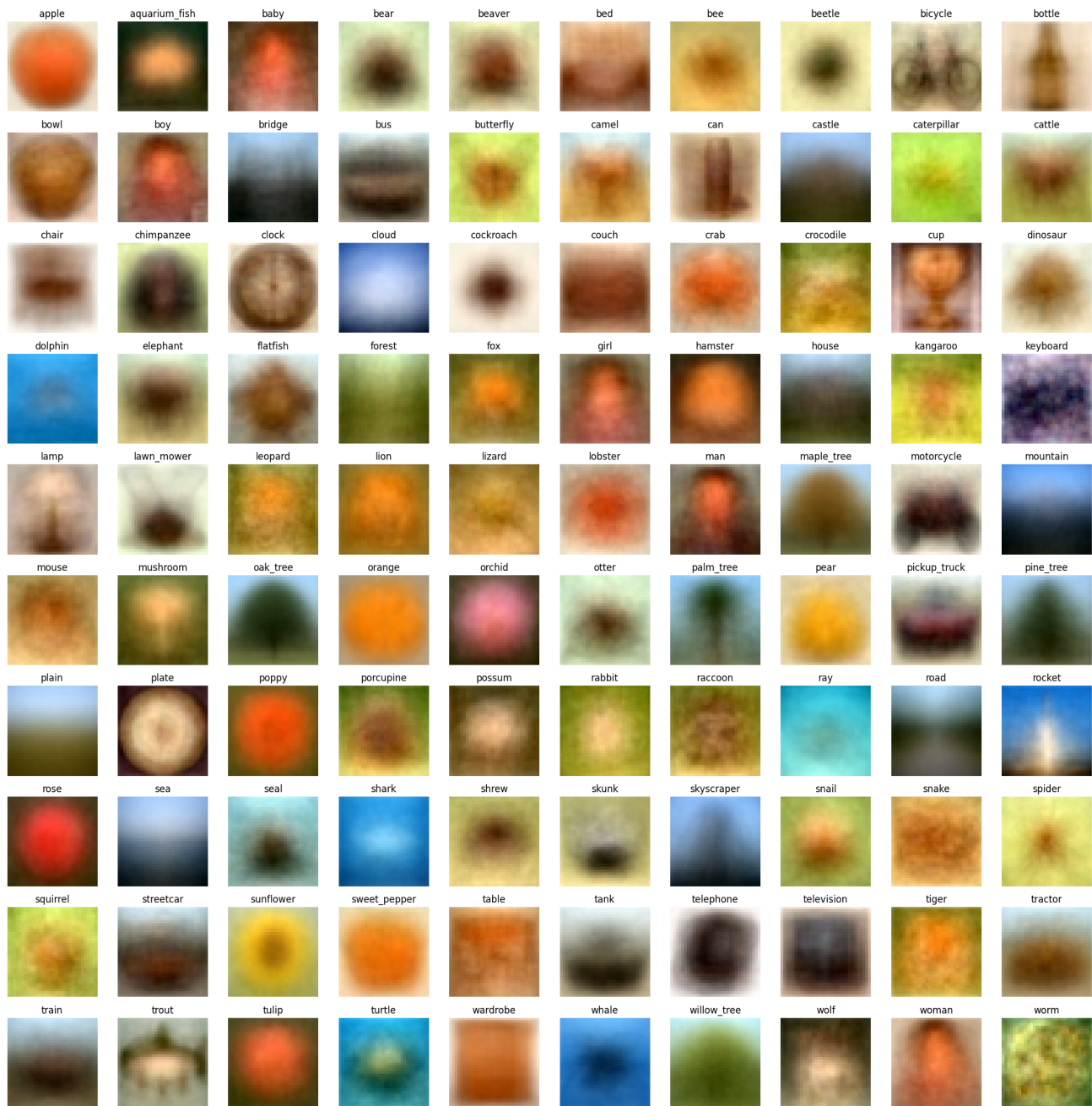


Figure 9. Average of all images within each class of Cifar100 dataset (all 100 classes).

11. More Experimental Results of Averaging on Weights V.S. Averaging on Features

The 2 models, 3 models, 5 models and 7 models for model merging/ensembling accuracy comparison between different architectures on Cifar100 are shown via Fig. 18, Fig. 19, Fig. 20 and Fig. 21, respectively. They all show that the models with ensembling on logits generally receive the best results and uniform soups receive the worst results. Besides, model-merging performs much

worse results for the ViT models and the gaps between uniform soups and ensemble on logits are enlarged with more models considered in.

Fig. 22 shows the performance gaps between ensembling on logits with greedy soups. From it, we can observe the similar phenomenon with the gaps of uniform soups, where the gaps grow when more models merged. But differently, the greedy soups break the going down trend as it can guarantee to maintain a relatively high accuracy level by only include the first model.

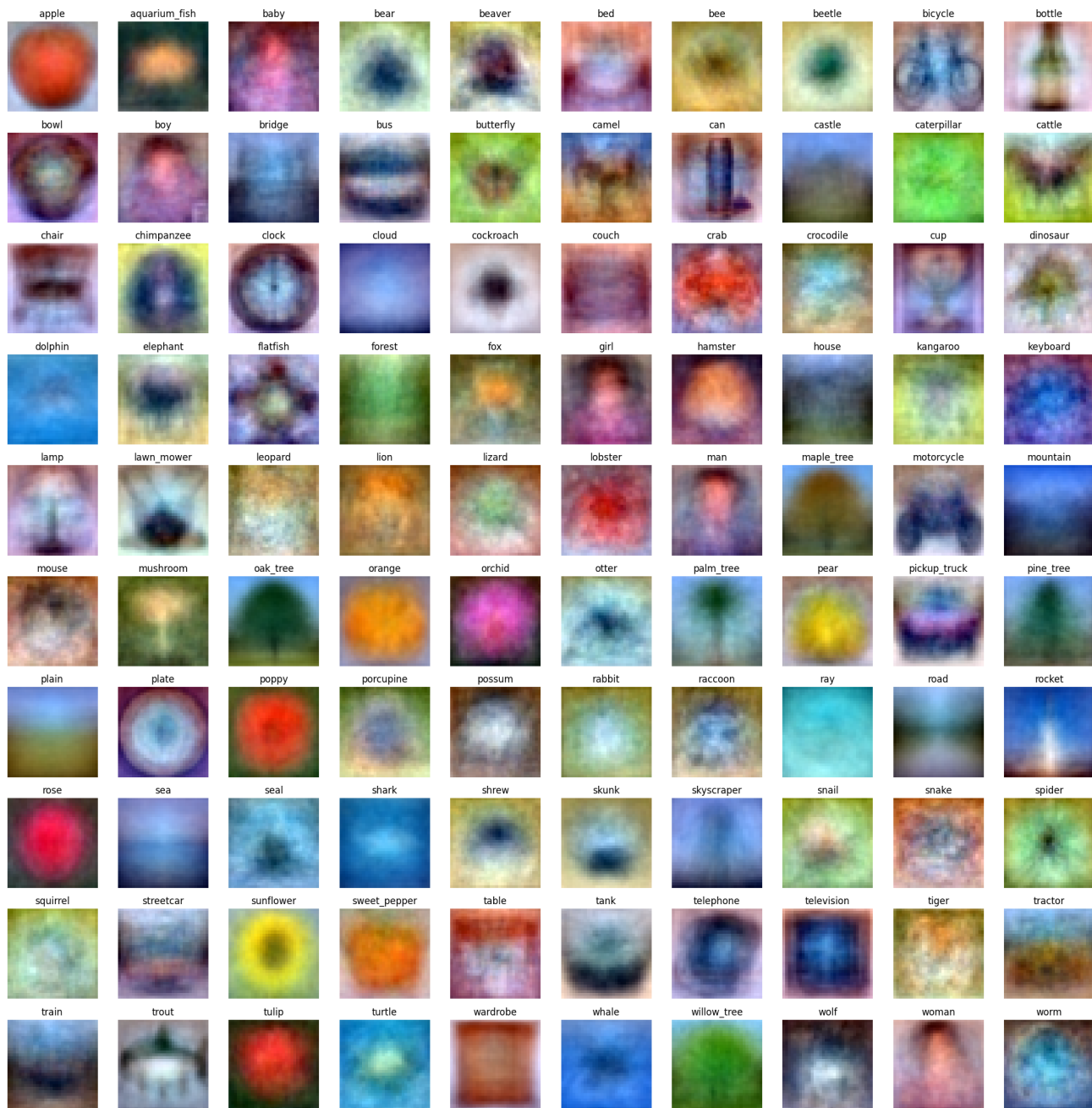


Figure 10. Linear classifiers visualization for each class of Cifar100 dataset (all 100 classes).

Also, we show the dataset-wise exploration of 2 models, 3 models, 5 models and 7 models merging/ensembling in Tab. 5, Tab. 6, Tab. 7 and Tab. 8, respectively. The computation consumptions in Floating Point Operations (FLOPs) and Parameter Numbers are in Tab. 9.

We illustrate the ViT model (DeiT Tiny) on another dataset — Tiny ImageNet in Tab. 10. We can also see the more models are merged, the worse results from uniform soups can get. Also, we can observe the greedy soups, greedy ensemble on logits and

greedy ensemble on features are not changed. It demonstrates the model-merging between 2 or more ViT models will not contribute to the performance. Thus, it shows the ViT models are not suitable for model-merging in the tested scenarios.

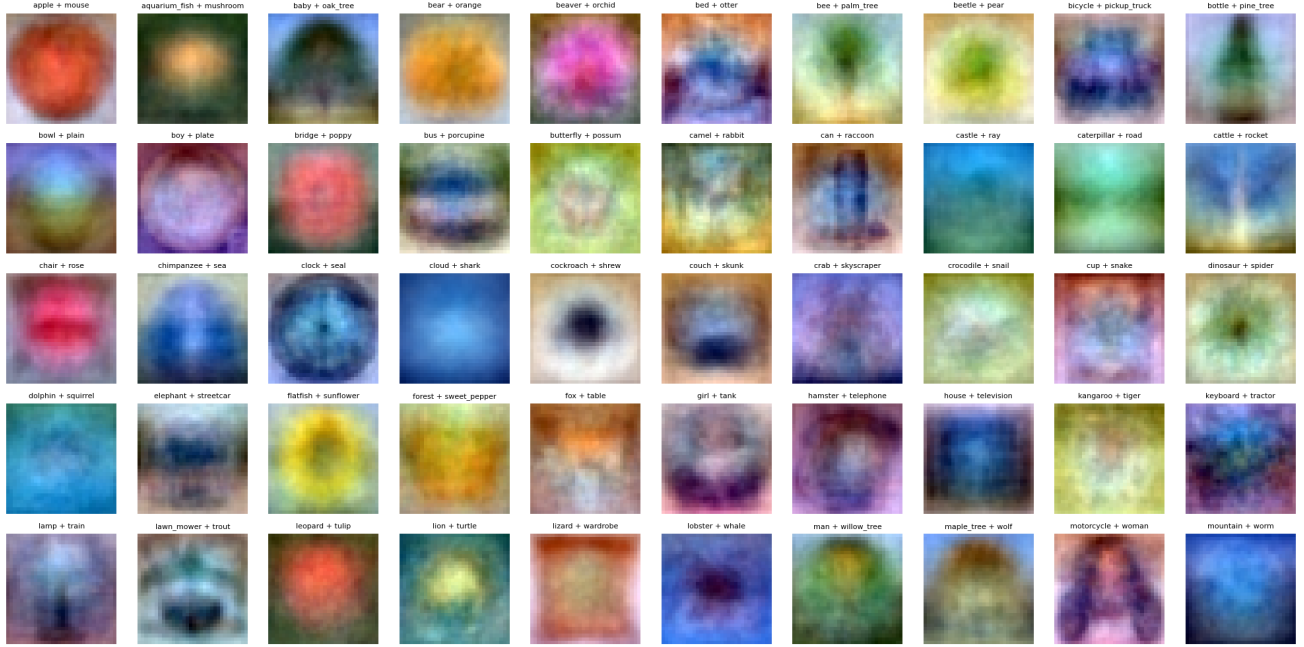


Figure 11. Merge the linear classifiers for the first 50 classes with the last 50 classes in Cifar100 dataset.

Table 5. Performance Comparison for VGG19 with 2 Models Across Different Datasets. For the ChestXRay dataset, We adopt averaged AUROC (Area Under Curve of Receiver Operating Characteristic) as the evaluation metric (normalized into 0 to 100 for better representation); while accuracy (0% to 100%) for the rest of datasets.

Datasets	Perf Ave	Uni Soups	Grd Soups	Ens Lgt	Ens Fts	Grd Ens Lgt	Grd Ens Fts
Cifar10	92.42	92.79	92.68	93.26	93.22	92.68	92.59
Cifar100	70.31	70.06	70.22	72.99	72.76	70.57	70.41
PathMNIST	89.75	40.85	88.41	91.60	82.06	88.61	88.47
DermaMNIST	74.19	71.97	73.57	74.66	72.72	73.87	73.57
Celeba	93.12	89.50	93.05	93.28	93.26	93.08	93.06
TinyImageNet	59.87	60.89	61.40	61.71	61.85	61.72	61.65
ChestXRay	80.52	79.80	80.43	81.14	80.85	80.43	80.43

Table 6. Performance Comparison for VGG19 with 3 Models Across Different Datasets. For the ChestXRay dataset, We adopt averaged AUROC (Area Under Curve of Receiver Operating Characteristic) as the evaluation metric (normalized into 0 to 100 for better representation); while accuracy (0% to 100%) for the rest of datasets.

Datasets	Perf Ave	Uni Soups	Grd Soups	Ens Logits	Ens Fts	Grd Ens Logits	Grd Ens Fts
Cifar10	92.47	92.82	92.65	93.54	93.48	92.75	92.65
Cifar100	70.34	69.80	70.14	73.85	73.49	70.29	70.40
PathMNIST	89.46	45.39	88.65	91.82	80.07	88.41	88.38
DermaMNIST	75.00	69.43	74.01	75.21	72.07	73.47	73.37
Celeba	93.12	77.69	93.12	93.31	93.30	93.01	93.06
TinyImageNet	59.85	61.39	61.55	62.40	62.41	62.60	62.61
ChestXRay	80.56	79.59	80.43	81.31	80.88	80.43	80.43

12. More Experimental Results of Model Magnitude Changes

The 2 models, 3 models, 5 models and 7 models accuracy vs. different magnification factors on Cifar100 are shown via Fig. 23,

ResNet50 Conv Layer 1 Kernels

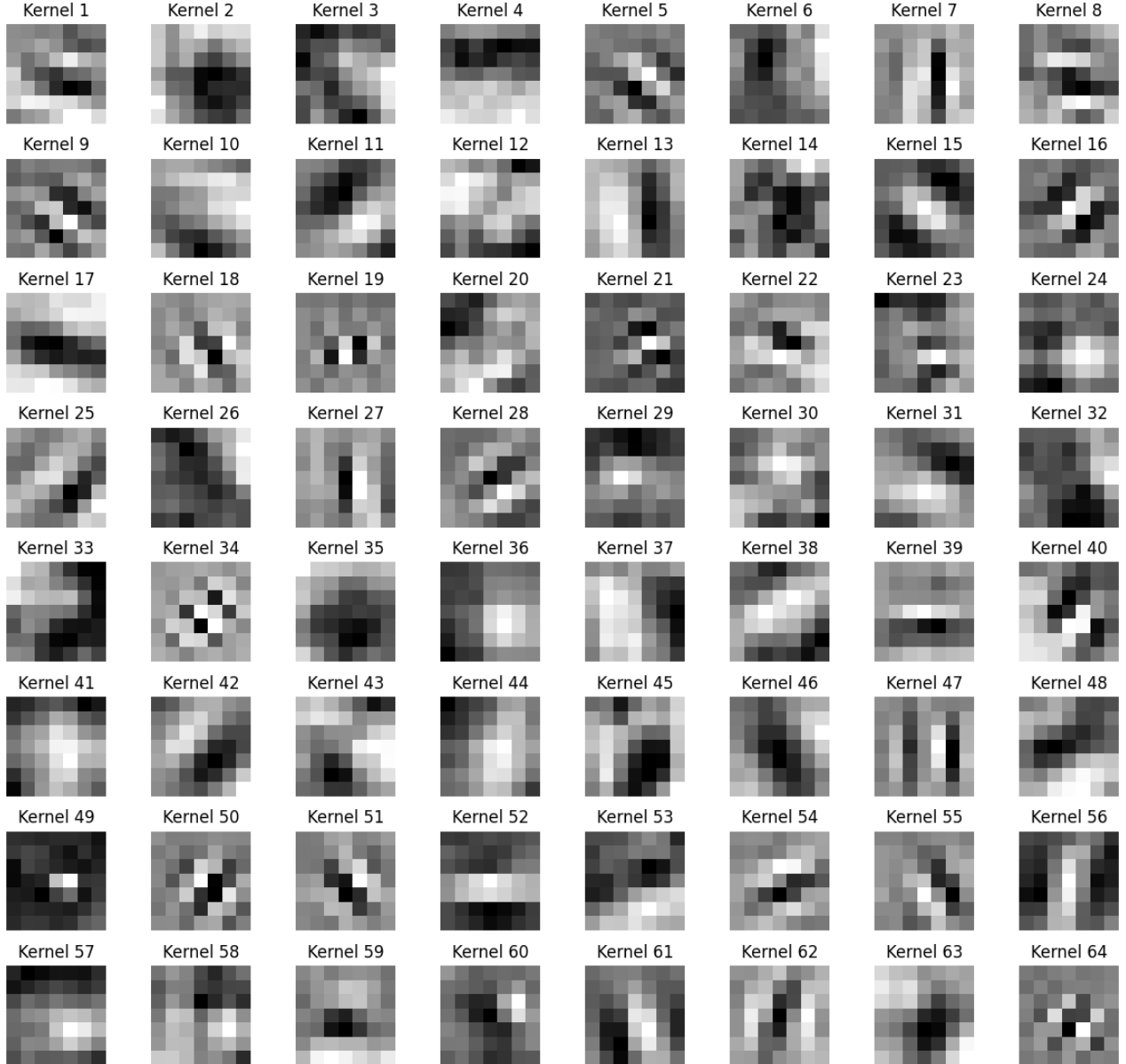


Figure 12. The first layer weights visualization of ResNet50.

Fig. 24, Fig. 25 and Fig. 26, respectively.

Similar to Cifar100, the 2 models, 3 models, 5 models, 7 models and 10 models accuracy vs. magnification factor on Cifar10 are shown via Fig. 27, Fig. 28, Fig. 29, Fig. 30 and Fig. 31, respectively. Moreover, we also visualize the uniform soup and logits ensemble accuracy vs. different magnification factors across different model numbers on the Cifar10 dataset in Fig. 32. We can observe similar phenomenons as discussed in the apepr. However, on the Cifar10, the gaps have different peak points than Cifar100,

which is $\times 110$ (for Cifar100, it is $\times 100$).

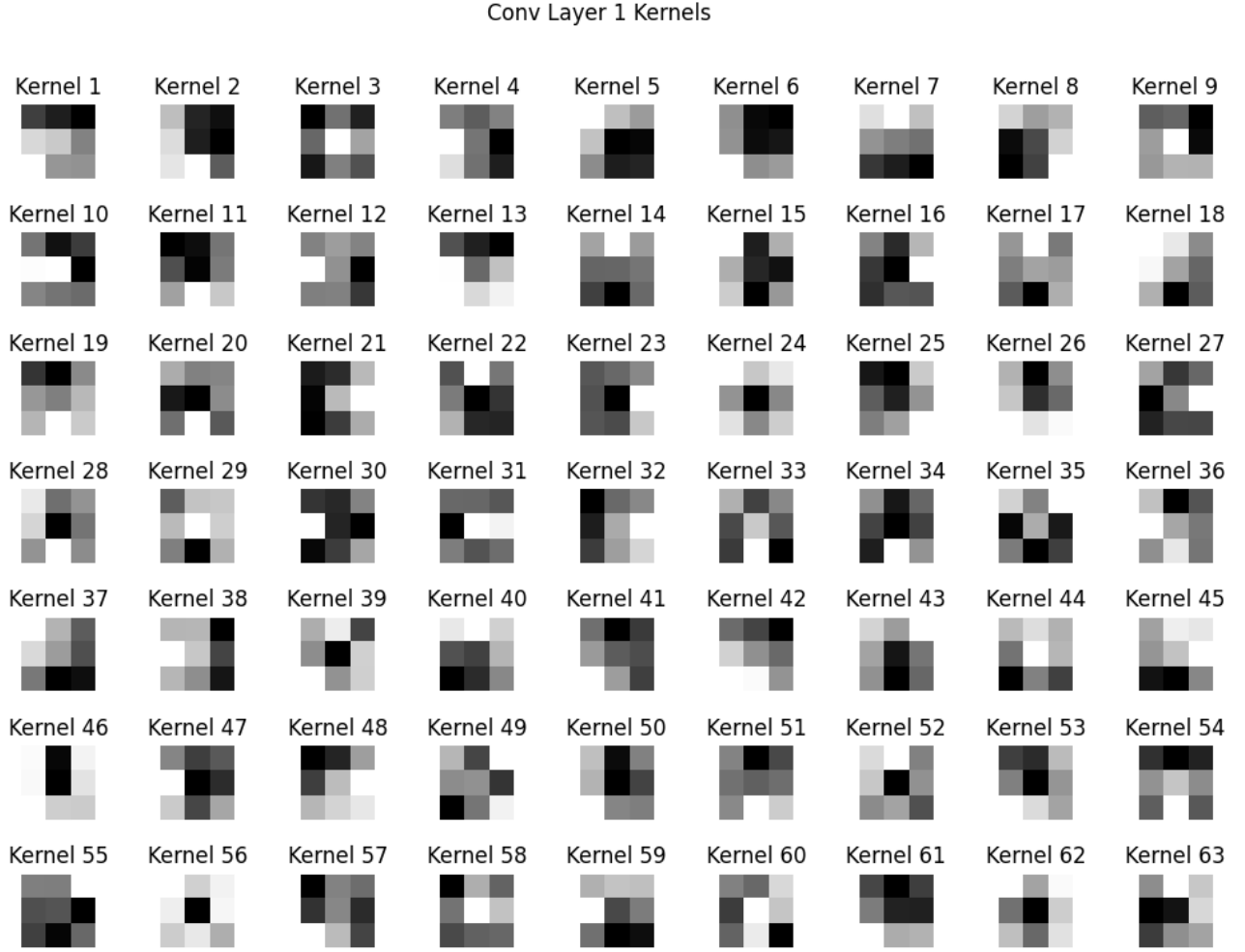


Figure 13. The first layer weights (first 63 conv kernels) visualization of VGG19.

Table 7. Performance Comparison for VGG19 with 5 Models Across Different Datasets. For the ChestXRay dataset, We adopt averaged AUROC (Area Under Curve of Receiver Operating Characteristic) as the evaluation metric (normalized into 0 to 100 for better representation); while accuracy (0% to 100%) for the rest of datasets.

Datasets	Perf Ave	Uni Soups	Grd Soups	Ens Logits	Ens Fts	Grd Ens Logits	Grd Ens Fts
Cifar10	92.45	92.90	92.65	93.70	93.71	81.95	92.65
Cifar100	70.47	69.73	70.32	74.90	74.18	70.35	70.31
PathMNIST	89.80	51.00	88.58	92.28	79.42	88.47	88.41
DermaMNIST	74.46	69.88	73.32	75.31	72.42	73.57	73.72
Celeba	93.03	60.27	93.06	93.45	93.32	93.06	93.04
TinyImageNet	59.89	61.55	61.91	63.08	63.17	63.29	63.27
ChestXRay	80.57	79.38	80.43	81.46	80.92	80.43	80.43

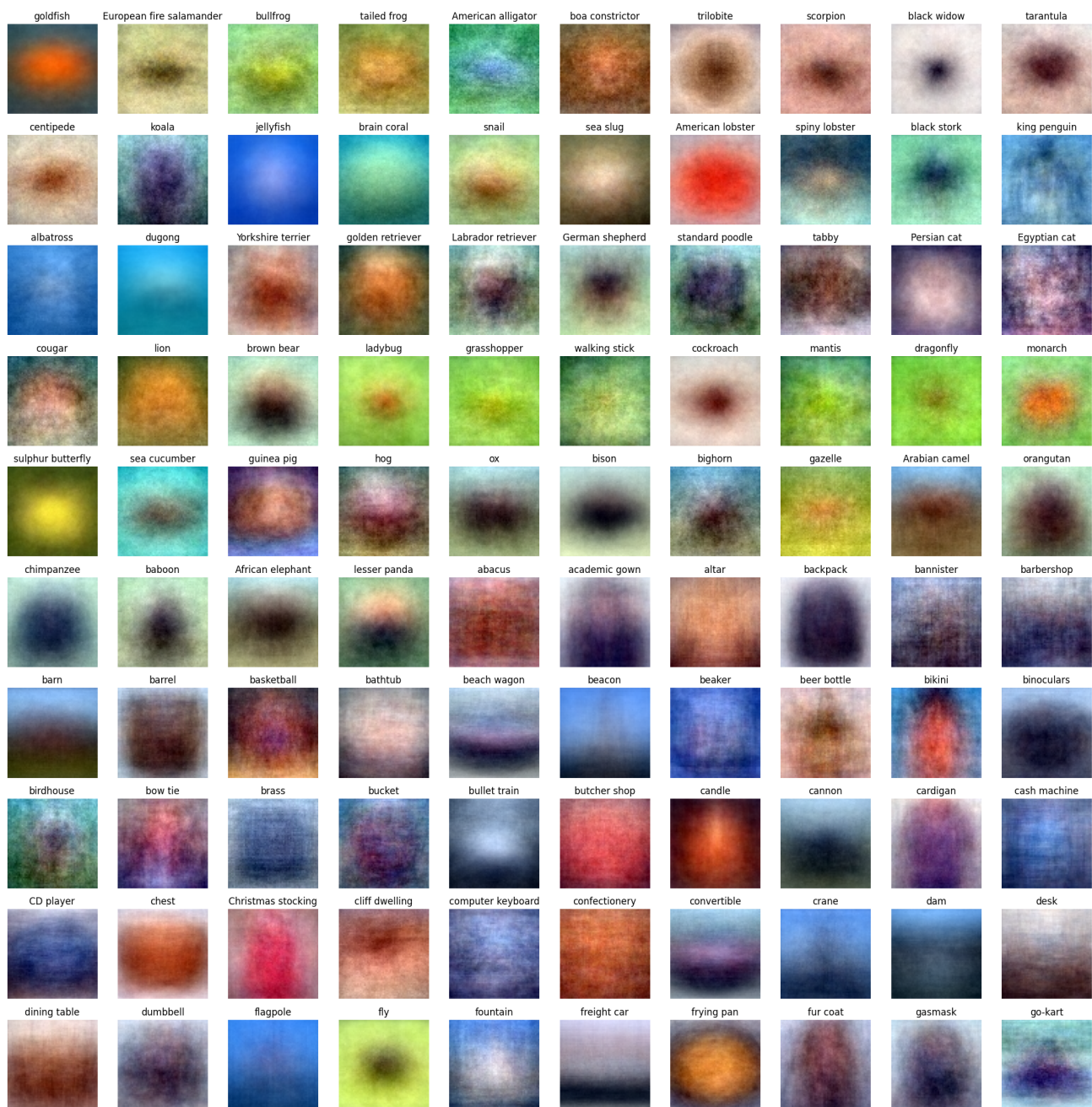


Figure 14. Average of all images within each class of TinyImageNet dataset (the first 100 classes).

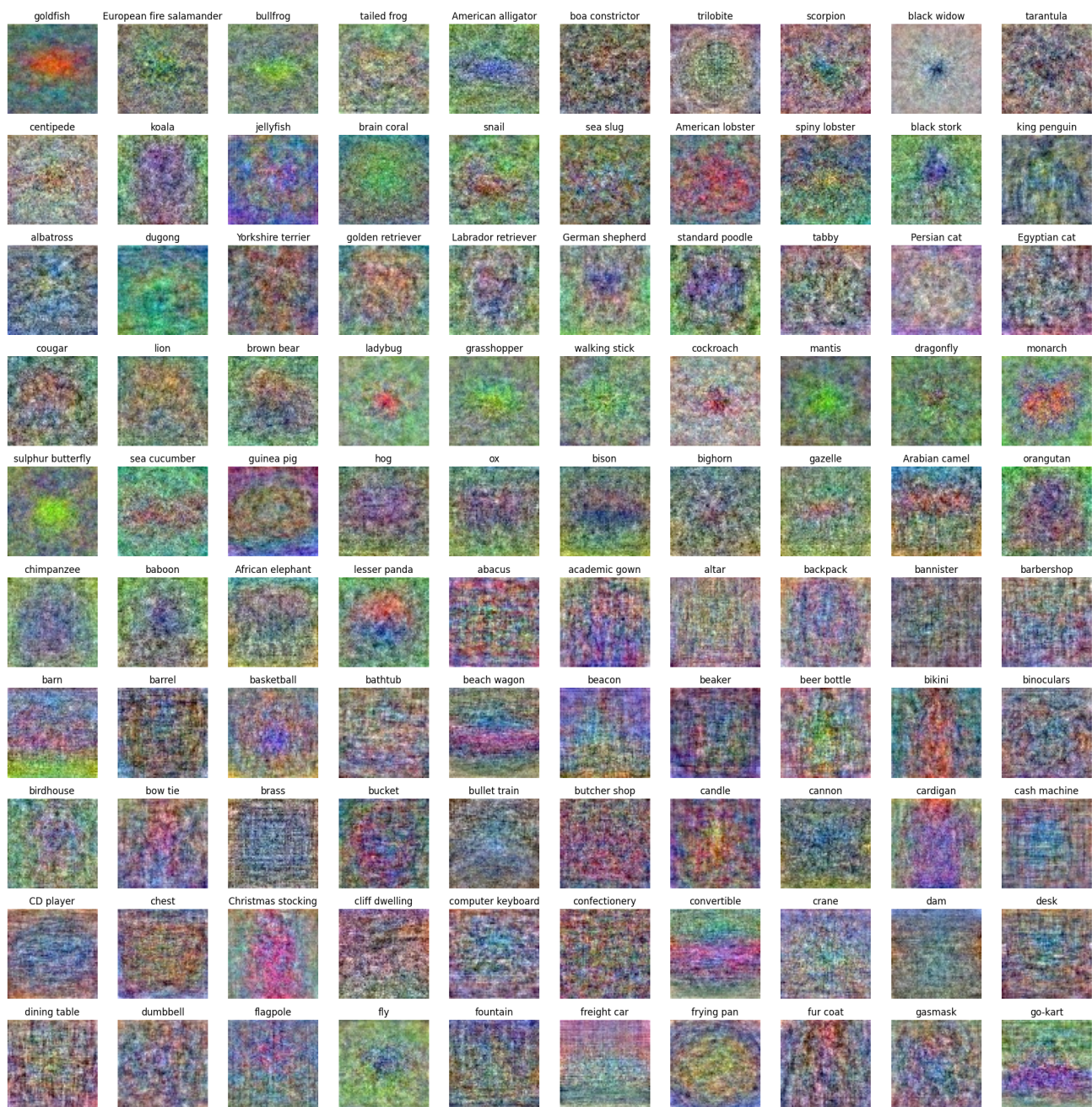


Figure 15. Linear classifiers visualization for each class of TinyImageNet dataset (the first 100 classes).

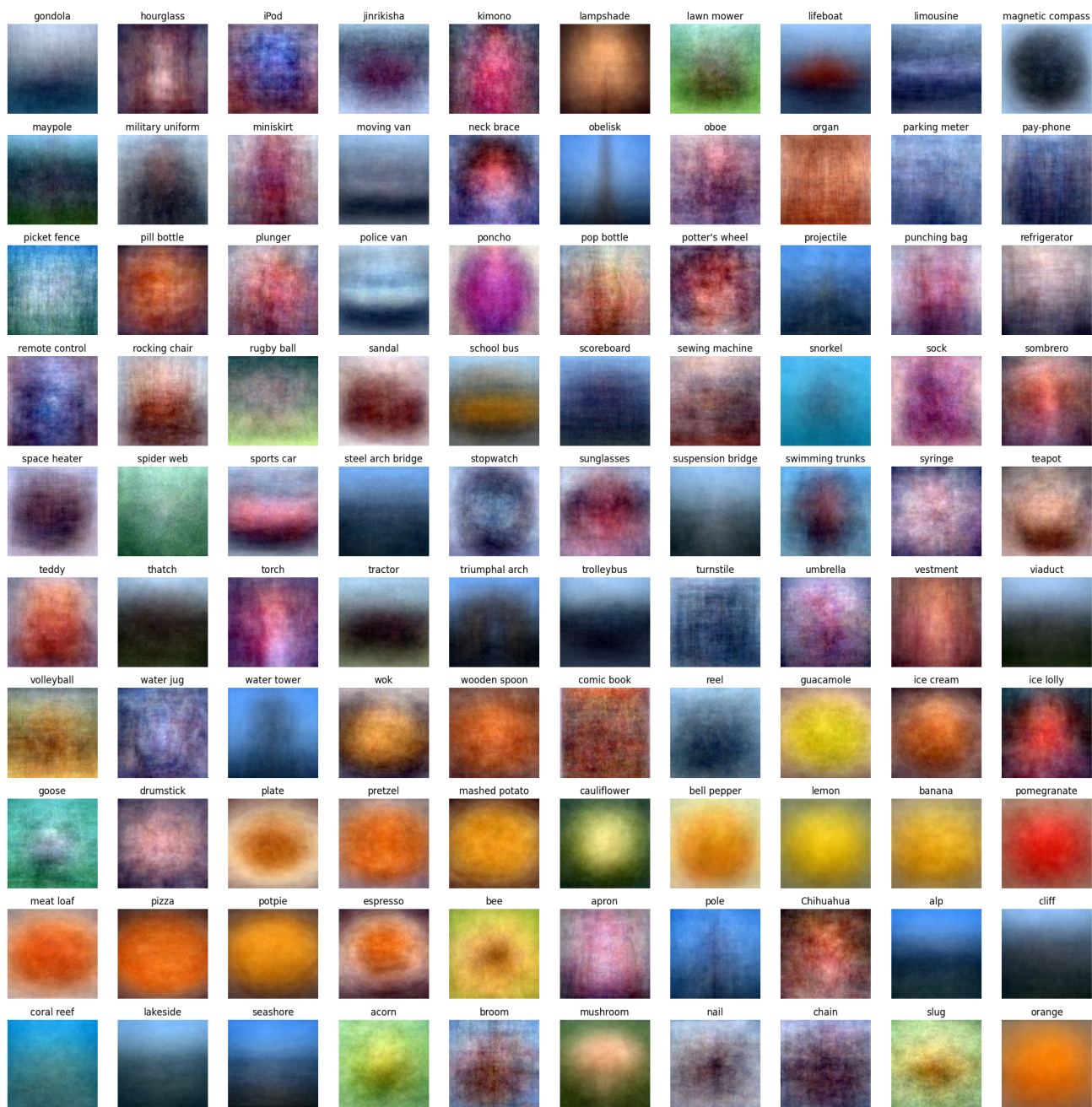


Figure 16. Average of all images within each class of TinyImageNet dataset (the last 100 classes).

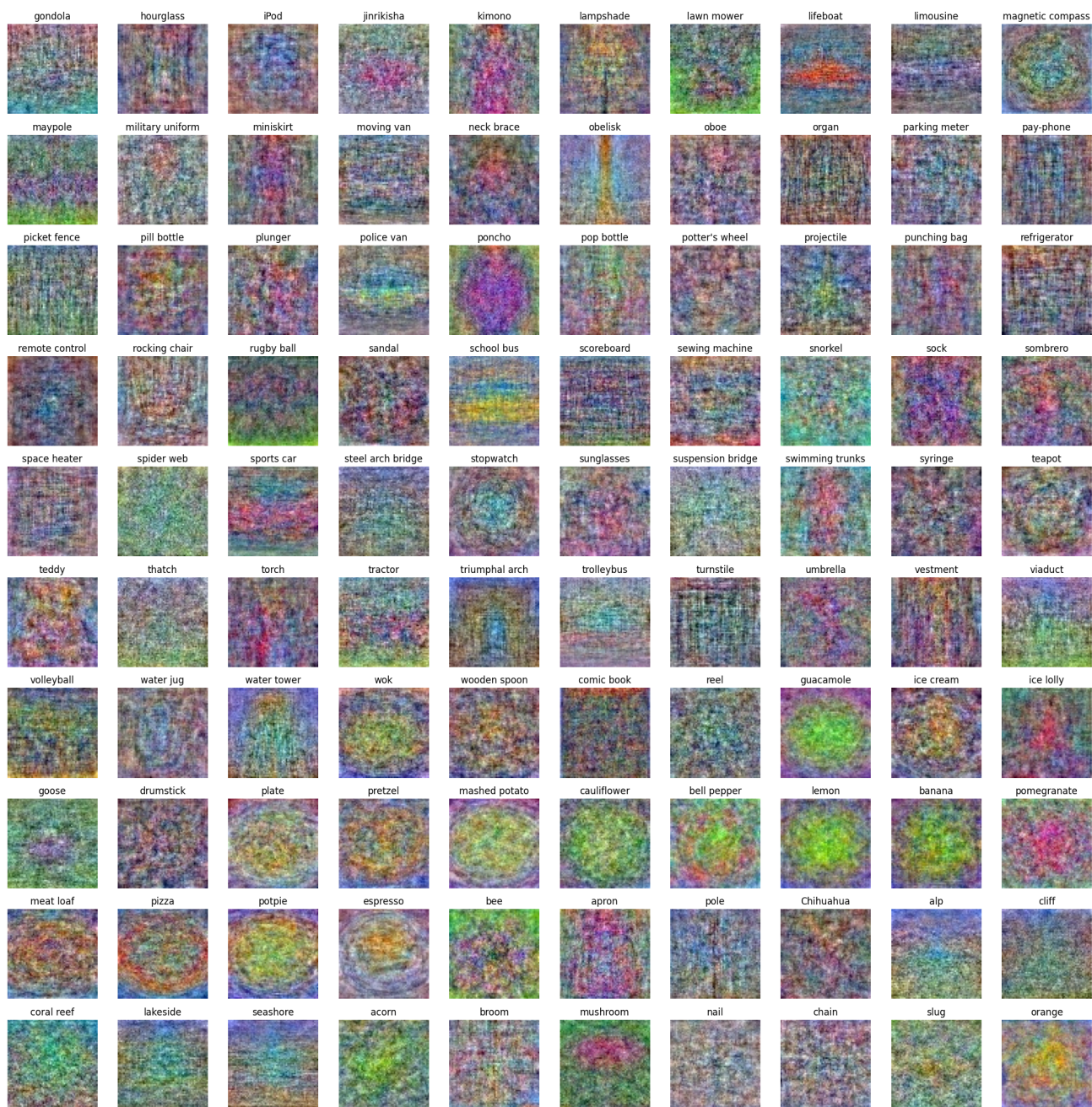


Figure 17. Linear classifiers visualization for each class of TinyImageNet dataset (the last 100 classes).

Table 8. Performance Comparison for VGG19 with 7 Models Across Different Datasets. For the ChestXRay dataset, We adopt averaged AUROC (Area Under Curve of Receiver Operating Characteristic) as the evaluation metric (normalized into 0 to 100 for better representation); while accuracy (0% to 100%) for the rest of datasets.

Datasets	Perf Ave	Uni Soups	Grd Soups	Ens Logits	Ens Fts	Grd Ens Logits	Grd Ens Fts
Cifar10	92.42	92.79	92.65	93.85	93.71	92.76	92.71
Cifar100	70.35	69.79	70.28	74.92	74.82	70.31	70.40
PathMNIST	89.66	38.76	88.44	92.48	79.97	88.50	88.54
DermaMNIST	74.12	69.83	73.67	75.86	70.57	73.82	74.06
Celeba	92.99	49.97	93.07	93.31	93.30	93.05	93.05
TinyImageNet	59.90	62.38	62.12	63.53	63.54	63.66	63.52
ChestXRay	80.60	79.22	80.43	81.61	80.99	80.43	80.43

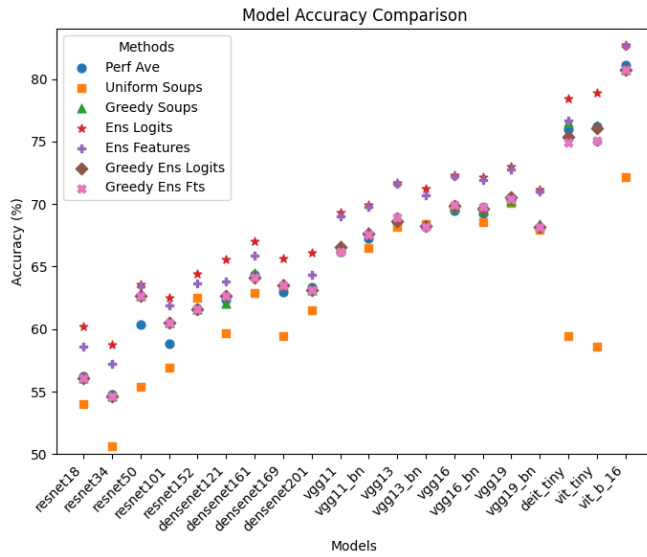


Figure 18. The 2 model merging/ensembling accuracy comparison between different architectures on Cifar100.

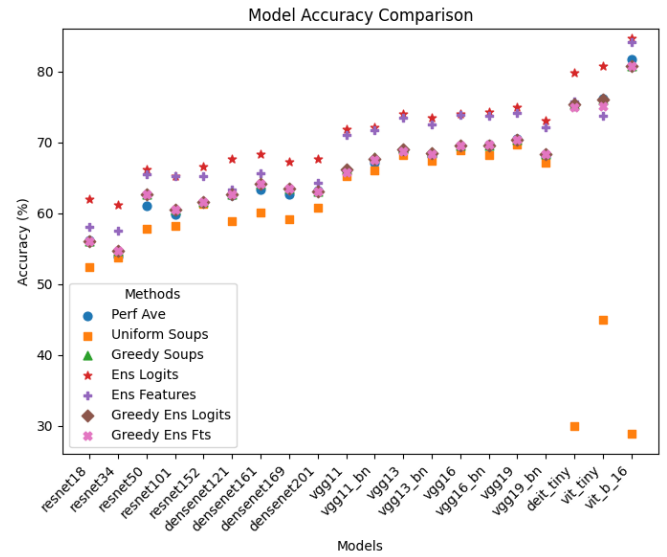


Figure 20. The 5 model merging/ensembling accuracy comparison between different architectures on Cifar100.

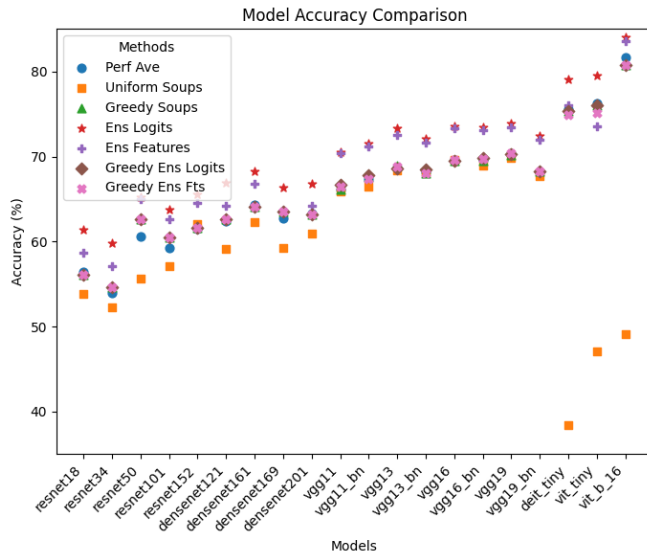


Figure 19. The 3 model merging/ensembling accuracy comparison between different architectures on Cifar100.

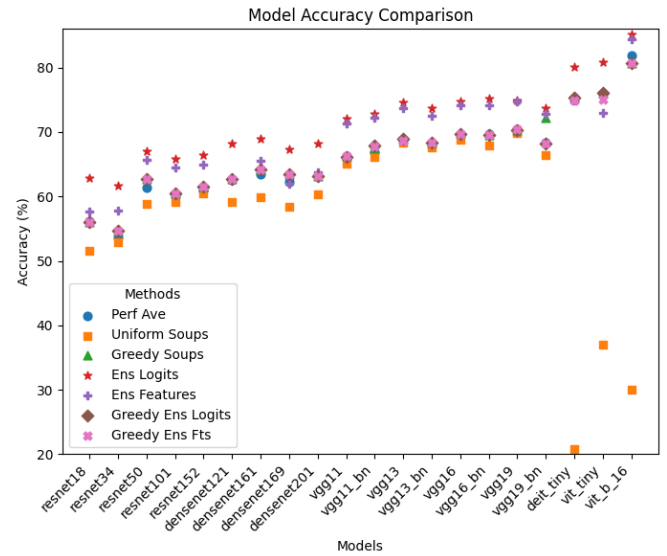


Figure 21. The 7 model merging/ensembling accuracy comparison between different architectures on Cifar100.

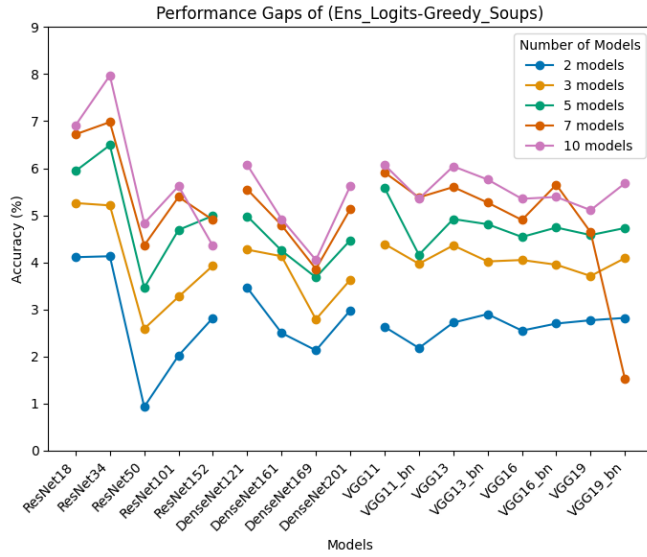


Figure 22. Performance Gaps between Logits Ensemble and Greedy Soups Across Different Configurations (excluded the ViT models as the scales are too different) on Cifar100.

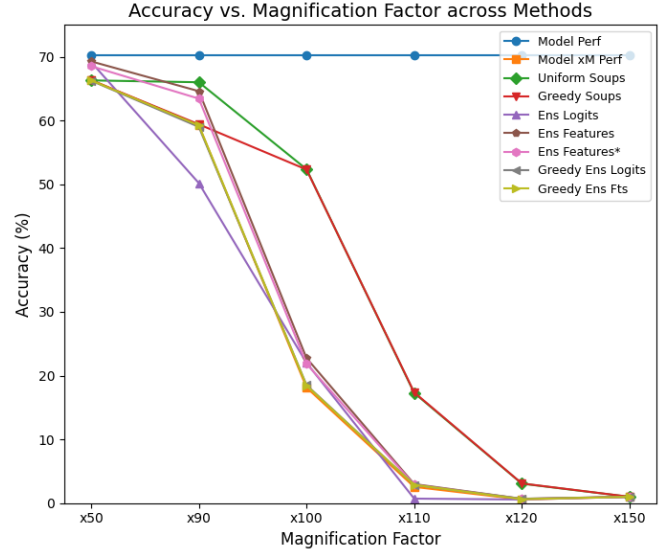


Figure 23. Accuracy vs. Magnification Factor across Methods with 2 models on Cifar100 dataset.

Table 9. Comparison of FLOPs and Parameter Numbers for Various Models. The FLOPs are calculated based on 224×224 for general purpose, e.g. ImageNet. “ViT_Tiny” denotes for “ViT_Tiny_Patch16_224” and “DeiT_Tiny” stands for “DeiT_Tiny_Patch16_224”, respectively.

Models	FLOPs (G)	Param # (M)
ResNet18	1.82	11.7
ResNet34	3.66	21.8
ResNet50	4.09	25.6
ResNet101	7.83	44.5
ResNet152	11.58	60.2
DenseNet121	2.88	8.0
DenseNet161	7.81	28.7
DenseNet169	3.36	14.3
DenseNet201	4.37	20.0
VGG11	7.63	132.9
VGG11_BN	7.76	132.9
VGG13	11.34	133.0
VGG13_BN	11.47	133.0
VGG16	15.5	138.4
VGG16_BN	15.52	138.4
VGG19	19.6	143.7
VGG19_BN	19.63	143.7
DeiT_Tiny	1.3	5.7
ViT_Tiny	1.3	5.7
ViT_B_16	17.6	86.4

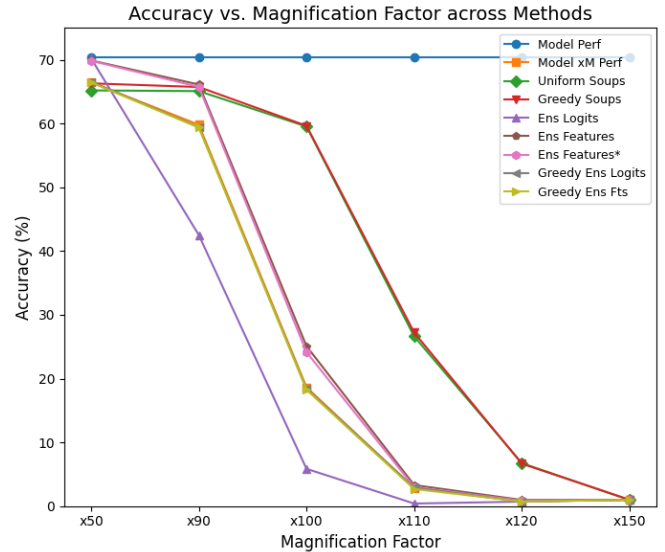


Figure 24. Accuracy vs. Magnification Factor across Methods with 3 models on Cifar100 dataset.

Table 10. Performance Comparison for DeiT on Tiny ImageNet Across Different Configurations. We adopt accuracy (0% to 100%) as the evaluation metric.

Model #	Perf Ave	Uniform Soups	Greedy Soups	Ens Logits	Ens Features	Greedy Ens Logits	Greedy Ens Fts
2 models	66.77	61.75	65.99	70.32	69.37	65.99	65.77
3 models	66.32	29.93	65.99	71.56	70.31	65.99	65.77
5 models	66.08	18.71	65.99	72.49	70.86	65.99	65.77
7 models	66.84	13.95	65.99	73.32	72.05	65.99	65.77
10 models	66.79	8.91	65.99	73.93	72.58	65.99	65.77

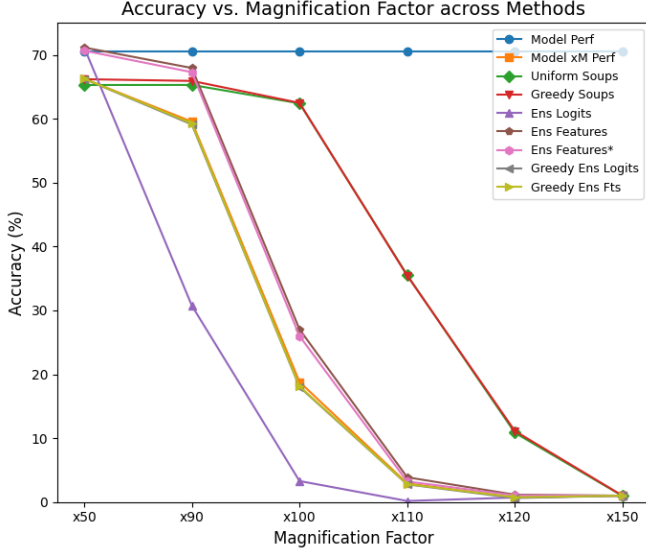


Figure 25. Accuracy vs. Magnification Factor across Methods with 5 models on Cifar100 dataset.

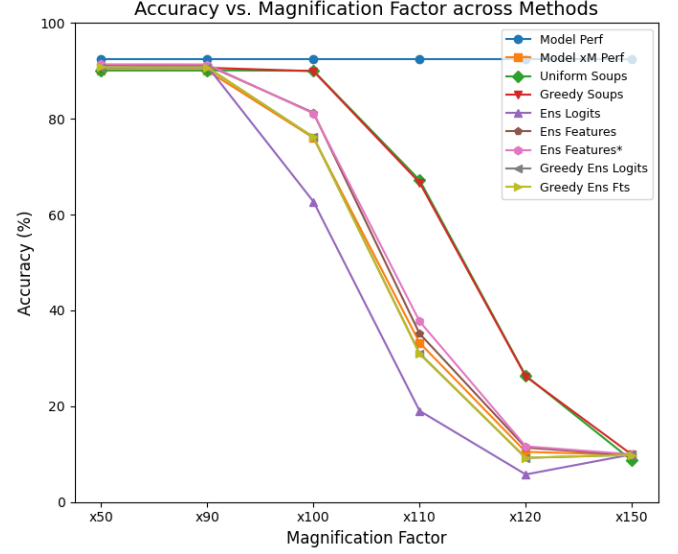


Figure 27. Accuracy vs. Magnification Factor across Methods with 2 models on Cifar10 dataset.

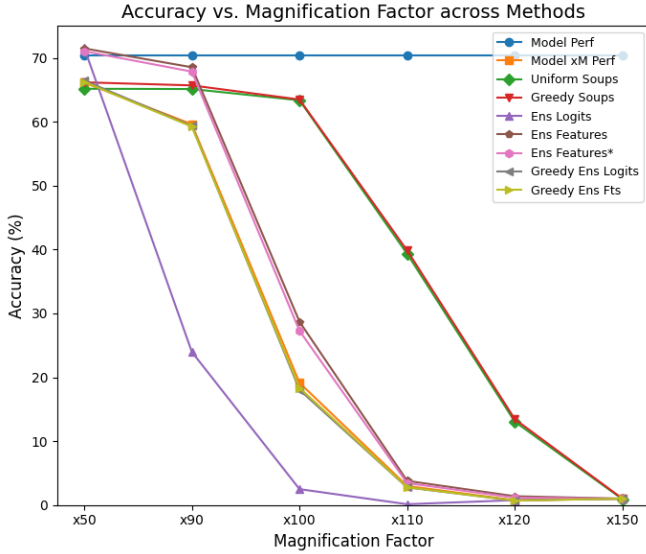


Figure 26. Accuracy vs. Magnification Factor across Methods with 7 models on Cifar100 dataset.

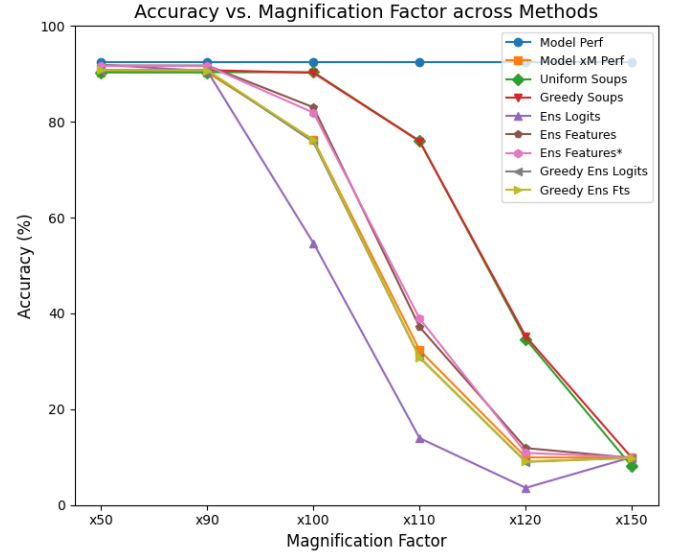


Figure 28. Accuracy vs. Magnification Factor across Methods with 3 models on Cifar10 dataset.

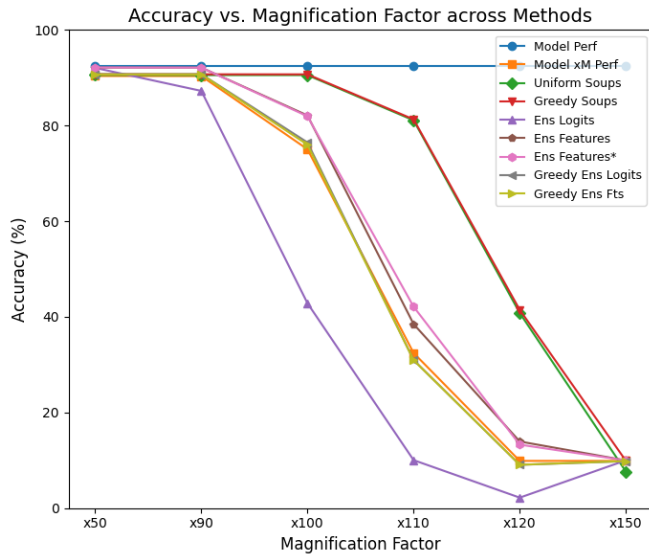


Figure 29. Accuracy vs. Magnification Factor across Methods with 5 models on Cifar10 dataset.

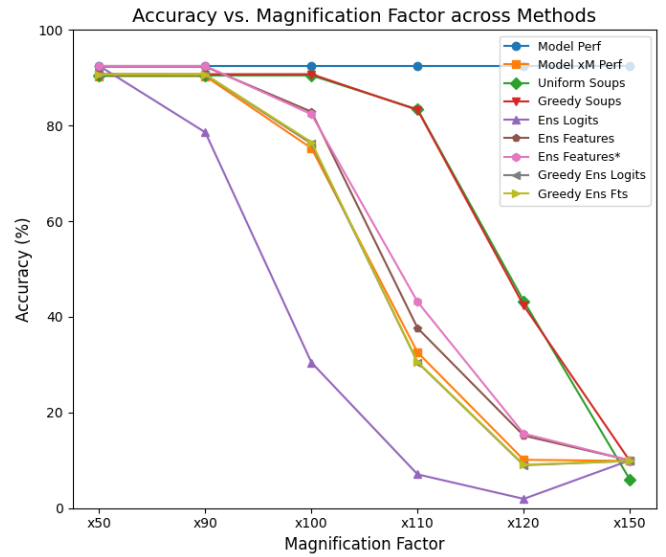


Figure 31. Accuracy vs. Magnification Factor across Methods with 10 models on Cifar10 dataset.

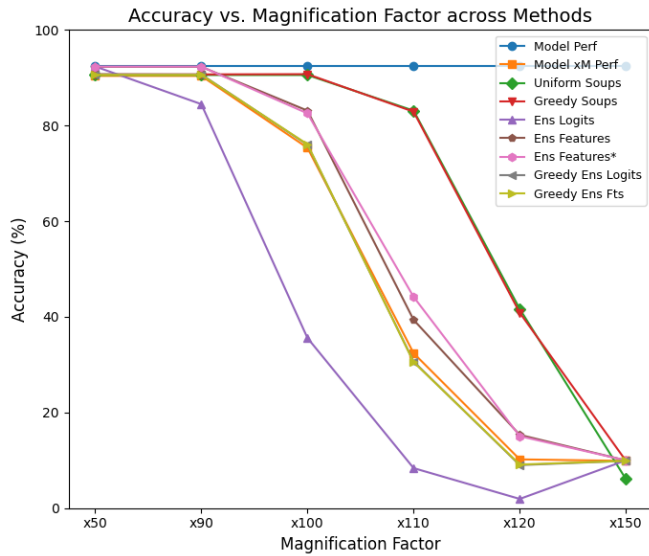


Figure 30. Accuracy vs. Magnification Factor across Methods with 7 models on Cifar10 dataset.

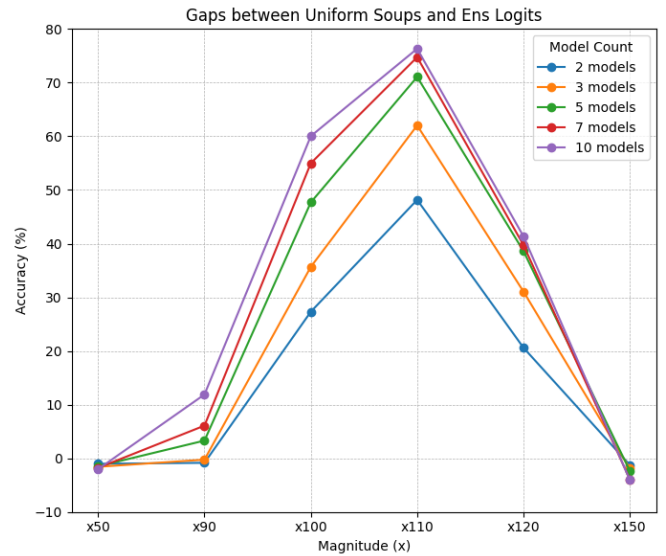


Figure 32. Uniform soup - Logits Ensemble Accuracy vs. Magnification Factor across different model numbers on Cifar10 dataset.